

STRETCHABLE 4-CHANNEL NECK RF COIL FOR 3T MRI

by

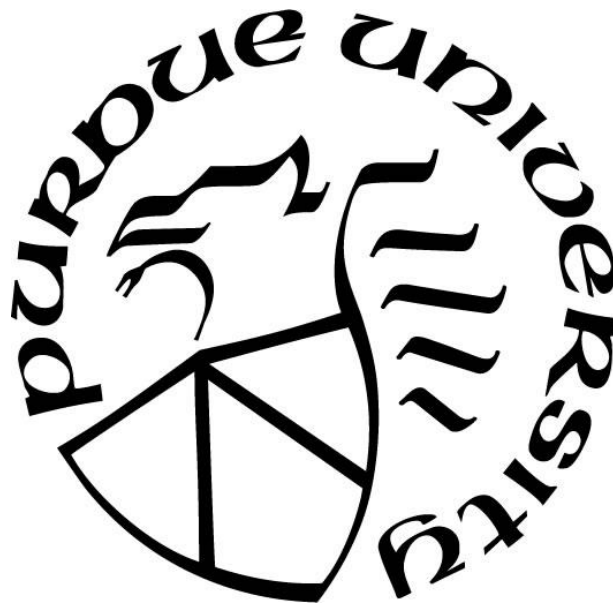
Minseon Gim

A Thesis

Submitted to the Faculty of Purdue University

In Partial Fulfillment of the Requirements for the degree of

Master of Science in Biomedical Engineering



Weldon School of Biomedical Engineering

West Lafayette, Indiana

August 2021

THE PURDUE UNIVERSITY GRADUATE SCHOOL
STATEMENT OF COMMITTEE APPROVAL

Dr. Joseph V. Rispoli, Chair

Weldon School of Biomedical Engineering

Dr. Yunjie Tong

Weldon School of Biomedical Engineering

Dr. Eric A. Nauman

School of Mechanical Engineering

Approved by:

Dr. Andrew O. Brightman

Dedicated to my parents, Jihui Yu and Byungjin Gim, for their support and encouragement.

ACKNOWLEDGMENTS

I would like to thank my advisor, Dr. Rispoli, for leading me throughout the years since undergraduate studies for guidance on radiofrequency (RF) coils and magnetic resonance imaging (MRI). With his mentorship, I learned not only numerous techniques, but also the attitude of being a good researcher. Whenever I faced an obstacle, he always helped me with great support and encouragement. I am also very thankful for my thesis committee members, Dr. Nauman and Dr. Tong, for their mentorship and guidance. All your supports encouraged me to accomplish the research.

I would also like to thank the Magnetic Resonance Biomedical Engineering Laboratory (MRBEL) members, especially Jana Vincent and Antonia Susnjar. Working in this lab was a wonderful opportunity for me. Lastly, I acknowledge the Weldon School of Biomedical Engineering. It was a luck to grow up in the supportive environment with a lot of opportunities.

TABLE OF CONTENTS

LIST OF TABLES	7
LIST OF FIGURES	8
ABSTRACT	11
1. INTRODUCTION	12
1.1 Magnetic Resonance Imaging	12
1.2 RF Coil	14
2. METHODS AND MATERIALS	16
2.1 Anthropometric Analysis	16
2.2 Stretchable Fabric	17
2.2.1 MRI Scan	17
2.2.2 Embroidery and Design	19
2.3 Conductive Thread	20
2.3.1 Impedance Measurement	20
2.4 Tuning and Matching Board	21
2.4.1 Printed Circuit Board Layout	21
2.4.2 Balun	22
2.4.3 Bench Measurement	24
2.4.4 Quality Factor	29
2.5 Dielectric Phantom	30
2.5.1 Dielectric Phantom Recipe	30
2.5.2 DAKS Measurement	31
2.6 MRI Scan	32
2.6.1 Method	32
3. RESULTS	36
3.1 Stretchable Coil	36
3.1.1 Specifications of the Coil	36
3.2 Bench Measurements	37
3.2.1 Balun	37
3.2.2 Dielectric Muscle Phantom Analysis	37

3.2.3	Coil Testing	39
3.3	MRI Analysis	43
3.3.1	Dielectric Phantom Scan.....	43
4.	CONCLUSION.....	47
	REFERENCES	48

LIST OF TABLES

Table 2.1 Neck circumference among 18- to 20-year-old volunteers [7]	16
Table 2.2 Midline and lateral neck length of male and female [8]	16
Table 2.3 Signal ROI and noise ROI values for 10 samples of stretchable fabrics	19
Table 2.4 Impedance of oval shaped and circle shaped frame in $R+jX$ form on Smith chart	21
Table 3.1 Theoretical and experimental values of relative permittivity and conductivity of the dielectric muscle phantom with the calculated percent error.....	38
Table 3.2 S_{21} measurement of the coil on the plastic bench with and without 5-V forward bias applied to the PIN diode trap	39
Table 3.3 S_{21} measurement of the coil on the dielectric phantom with and without 5-V forward bias applied to the PIN diode trap	39
Table 3.4 Quality factors from the unloaded and loaded measurements. Ratio refers to the unloaded to the loaded.	42
Table 3.5 SNR calculations for axial T1, axial IDEAL, and sagittal T2-weighted images.....	46

LIST OF FIGURES

Figure 1.1 Signal intensities in T1-weighted image [3].....	12
Figure 1.2 Signal intensities in T2-weighted image [3].....	13
Figure 1.3 T1 and T2-weighted scan comparison on brain tumor [3]	13
Figure 1.4 The basic components of MRI system [5].....	14
Figure 1.5 Signal-to-noise ratio (SNR) improvement obtained by using different size coil arrays as compared to a single coil with the same overall dimension. All coils were modeled as being 1 cm over a lossy half-plane consisting of 0.72 S/m saline. SNR data was calculated on a line perpendicular to the coil plane and over the center of the array. [6]	15
Figure 1.6 Calculated (a) and measured (b) results comparing the SNR of a 16-channel head coil, a single element in the array, and a standard quadrature head coil [6]	15
Figure 2.1 Reference line for neck length measurement. Midline neck length (MNL) was measured from the upper margin of the hyoid bone to the jugular notch. Lateral neck length (LNL) was measured from the mandibular angle to the mid-portion of the ipsilateral clavicle. [8]	17
Figure 2.2 Example of signal ROI and noise ROI measurement.....	18
Figure 2.3 Outline of stitch pattern with hook-and-loop anchors	20
Figure 2.4 Oval (left) and circle (right) frames used for the impedance measurements	21
Figure 2.5 Example PCB board layouts in EAGLE software.....	22
Figure 2.6 Sample printed PCB board	22
Figure 2.7 Bench setup of the S_{21} measurement for tuning a balun	23
Figure 2.8 Example S_{21} measurement of the balun with 27-pF capacitor	23
Figure 2.9 Schematic of the RF coil connected to the tuning and matching capacitors only. C1 and C2 are matching capacitors, and C3 and C4 are tuning capacitors. C2 and C3 are variable capacitors to adjust capacitance. C3 and C4 have equal capacitance.	24
Figure 2.10 S_{21} measurement with coil, as indicated in Figure 2.9, and single-loop probe	25
Figure 2.11 Schematic of the RF coil connected to the final tuning and matching board including inductor and diode. C_m is for matching and C_t is for tuning. The dashed region is the trap comprised of L, C, and D.....	25
Figure 2.12 Pre-adjustment of the active detuning trap using a sniffer probe	26
Figure 2.13 S_{11} (yellow) and S_{21} (cyan) measurements of the active detuning trap.....	26
Figure 2.14 S_{21} measurement with an overlapped double-loop probe on a dielectric muscle phantom.....	27

Figure 2.15 Setup of the S_{21} measurement loaded with the muscle phantom.....	28
Figure 2.16 S_{21} measurement of the tuned state (diode off) and dip of the detuned state (diode on) of channel 1 on the plastic bench.	28
Figure 2.17 Q-factor showing the peak and -3dB points [11]	29
Figure 2.18 Example automated Q-factor measurement on the network analyzer	30
Figure 2.19 Photograph of cylindrical muscle-mimicking dielectric phantom	31
Figure 2.20 Process of DAKS measurements. The DAK-12 (SPEAG) was attached with R60 Vector Reflectometer (Copper Mountain Technologies) to measure the permittivity and the conductivity of the dielectric phantom.	32
Figure 2.21 Abdominal image scanned with IDEAL sequence [16]	33
Figure 2.22 Regions of noise (yellow) and regions of signal (numbered) used for the SNR calculation in the axial T1 image. Signal region 1 is the gap between the coil near the surface of the phantom, 2 is the center of the phantom, 3 is the center of coil near the surface of the phantom.	34
Figure 2.23 Regions of noise (yellow) and regions of signal (numbered) used for the SNR calculation in the sagittal T2 image. Signal region 1 is the center of the phantom, 2 is the center of the coil near the surface of the phantom.	35
Figure 3.1 Zigzag stitch pattern dimensions	36
Figure 3.2 LYO332Ag stitched on the stretchable fabric in zigzag pattern	36
Figure 3.3 Relative permittivity of the dielectric muscle phantom measured using DAKS.....	37
Figure 3.4 Conductivity of the dielectric muscle phantom measured using DAKS	38
Figure 3.5 S_{21} measurement of the coil on the dielectric phantom with and without 5-V forward bias applied to the PIN diode trap for the channel 1	40
Figure 3.6 S_{21} measurement of the coil on the dielectric phantom with and without 5-V forward bias applied to the PIN diode trap for the channel 2.....	40
Figure 3.7 S_{21} measurement of the coil on the dielectric phantom with and without 5-V forward bias applied to the PIN diode trap for the channel 3.....	41
Figure 3.8 S_{21} measurement of the coil on the dielectric phantom with and without 5-V forward bias applied to the PIN diode trap for the channel 4.....	41
Figure 3.9 Q-factor measurement of the channel 2 on the plastic bench.....	42
Figure 3.10 Q-factor measurement of the channel 2 on the dielectric phantom.....	43
Figure 3.11 Axial T1-weighted MRI scan. Brightness and windowing were adjusted to accentuate the brightness near the coil.	44

Figure 3.12 IDEAL T1-weighted MRI scan. Brightness and windowing were adjusted to accentuate the brightness near the coil. IDEAL sequence includes water only, fat only, in-phase, and out-of-phase sequences. 45

Figure 3.13 Sagittal T2-weighted MRI scan. Brightness and windowing were adjusted to accentuate the brightness near the coil..... 46

ABSTRACT

Advancements on flexible radiofrequency (RF) coils have been made to accommodate a variety of body sizes with great image quality and a comfortable imaging process. RF coils are magnetic field antennas for magnetic resonance imaging (MRI) that broadcast the RF signal to the patient and receive the returning signal to affect the image quality. The conventional neck RF coil is rigid and requires the patients to be in supine position. Due to its characteristics, the patients who have difficulties to move their neck experience an uncomfortable imaging process. The novel 4-channel neck RF coil is made of conductive silver thread embroidered on stretchable fabric to provide patients a more comfortable experience with lightweight and flexible materials. A wide range of neck sizes can be covered with the stretchable materials and great image quality can be acquired due to the RF coil positioned close to the source. The stretchable RF coil was built as non-overlapping 4 channels in zigzag stitch pattern and tested on a dielectric phantom, which was made to have the permittivity and conductivity of muscle at 128 MHz. The research can be extended to stretchable RF coils with more channels and different stitching patterns. It also has potential to be applied on joints such as wrist and ankle due to its flexibility to cover the curved surface.

1. INTRODUCTION

1.1 Magnetic Resonance Imaging

Magnetic resonance imaging (MRI) is a non-invasive technique to generate images of the organs and tissues of the body via magnetic field. Considering the body is composed of more than 60% of water, MRI utilizes its hydrogen protons. When the patient is in the MRI scanner, the hydrogen protons spin and align along with the direction of the magnetic field, and the magnetic vector deflects when additional radiofrequency energy is added. The protons return to their original spin when the radiofrequency energy is turned off, and the process creates signal that can be called MR images.

1.5T and 3T are the most common MRI machines in clinical settings. Of these, 3T has advantages of acquiring faster scan speed and better image quality through improved signal-to-noise ratio (SNR) compared to the 1.5T. These aspects allow 3T MRI to be more accessible in not only research, but also clinical settings. Due to its significance, the research is designed for 3T to consider further applications [1].

The most common MRI sequences are T1-weighted and T2-weighted scans. T1-weighted scan has shorter echo time (TE) and repetition time (TR) compared to T2-weighted scan. T1-weighted image displays fat, protein, blood, and gadolinium in bright color to map the proton energy within the fatty tissues of the body. In comparison, T2-weighted image displays fluid, CSF, and kidneys in bright color to map the proton energy within fatty and water-based tissues of the body [2] (Figure 1.1 - 1.3).

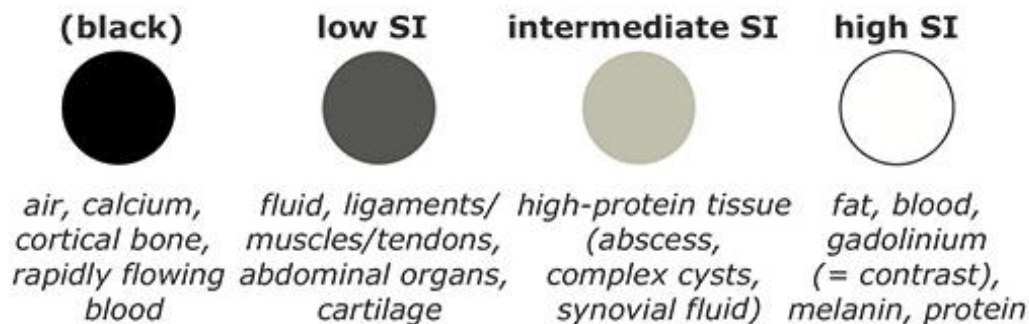


Figure 1.1 Signal intensities in T1-weighted image [3]




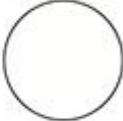
(black)	low SI	intermediate SI	high SI
			
<i>air, calcium, cortical bone, rapidly flowing blood</i>	<i>ligaments, tendons, liver, pancreas, adrenals, cartilage</i>	<i>fat, liver, pancreas, adrenals, muscles, cartilage</i>	<i>fluid, CSF, bladder, bile/ gallbladder, kidneys</i>

Figure 1.2 Signal intensities in T2-weighted image [3]

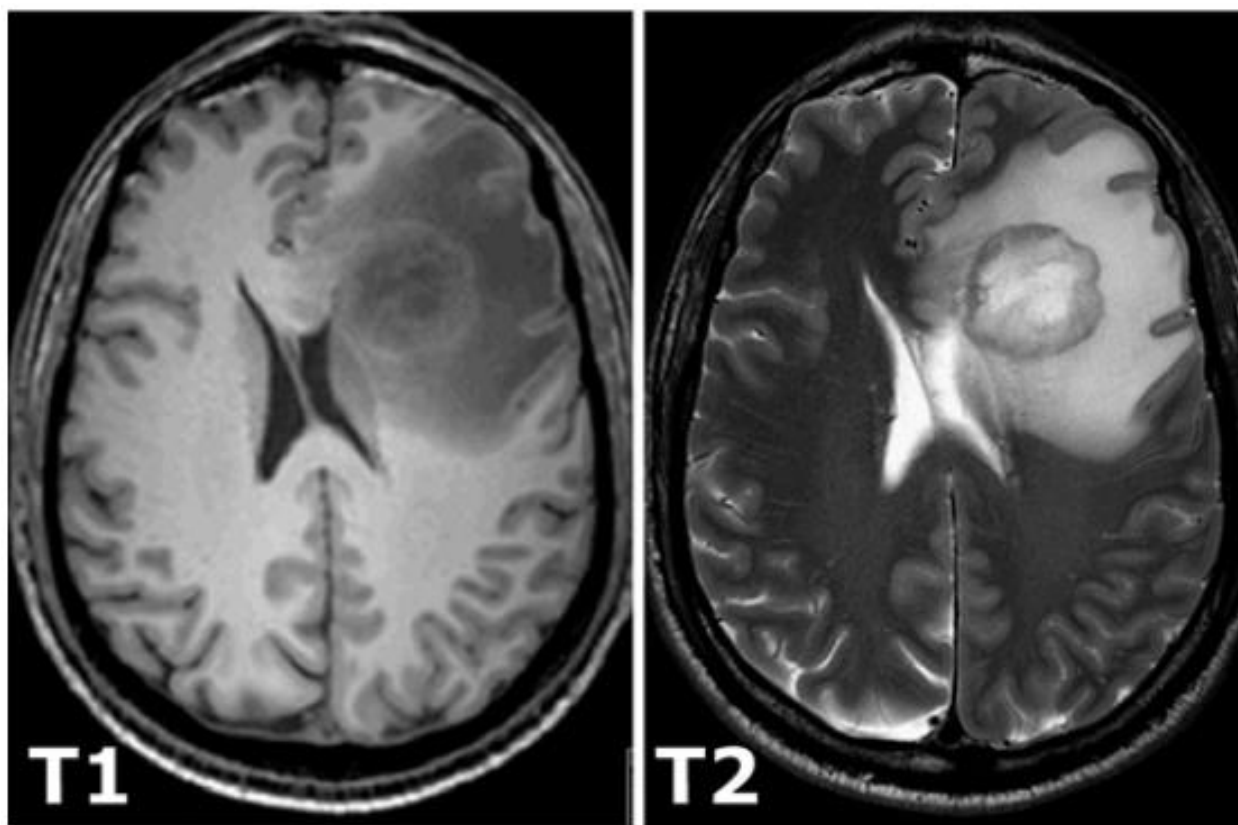


Figure 1.3 T1 and T2-weighted scan comparison on brain tumor [3]

1.2 RF Coil

A radiofrequency (RF) coil is the antenna of the MRI process. It broadcasts the RF signal to the patient and/or receives the returning signal [4]. With its characteristics, an RF coil can be used as a transmitter, receiver, or both. The main role as a transmitter is generating an RF magnetic field, and the main role as a receiver is detecting the nuclear magnetic resonance signal.

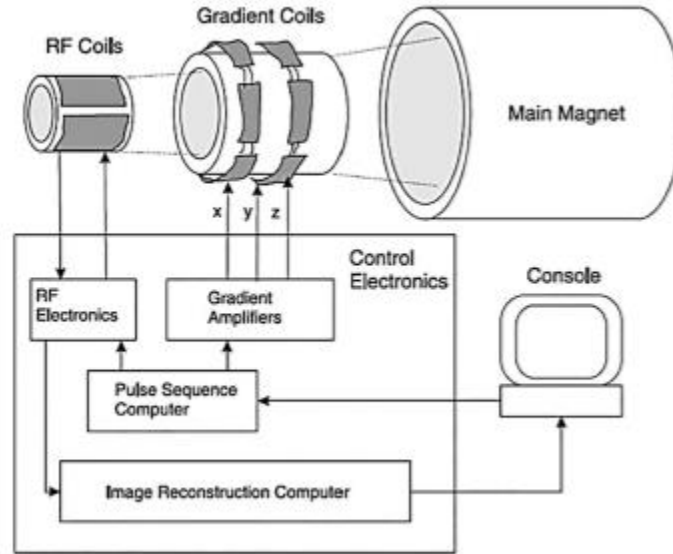


Figure 1.4 The basic components of MRI system [5]

As shown in Figure 1.4, the main magnet produces B_0 field to align the spins and the gradient coils enable image encoding in all three directions of x, y, z. The RF coil excites the aligned spins and receives the RF signal from the source. As RF coil transmits and receives the signal, the RF receive coil detects the magnetization resulted in an electric current via electromagnetic induction [5].

As the signal-to-noise ratio (SNR) represents the ratio of the signal voltage to the noise voltage, the SNR near the center of the phantom is lower than the surface. The research regarding the SNR improvements in phased arrays shows the relationship between the SNR and the distance from the center of the subject on Figure 1.5 and 1.6 [6].

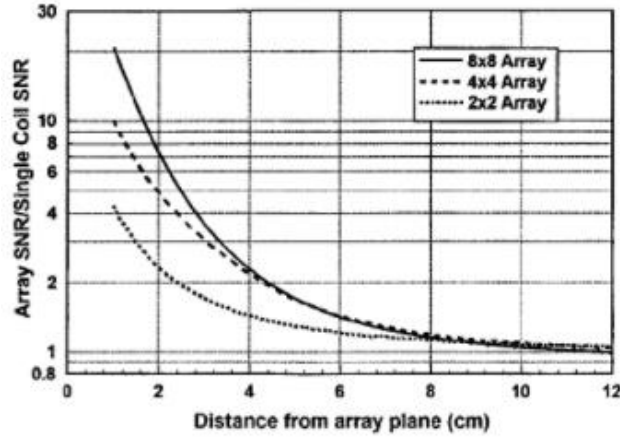


Figure 1.5 Signal-to-noise ratio (SNR) improvement obtained by using different size coil arrays as compared to a single coil with the same overall dimension. All coils were modeled as being 1 cm over a lossy half-plane consisting of 0.72 S/m saline. SNR data was calculated on a line perpendicular to the coil plane and over the center of the array. [6]

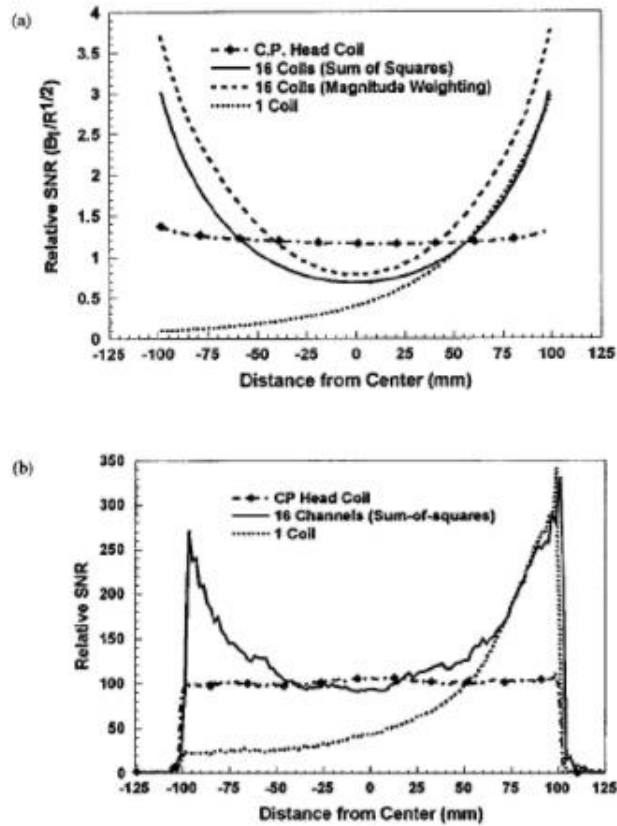


Figure 1.6 Calculated (a) and measured (b) results comparing the SNR of a 16-channel head coil, a single element in the array, and a standard quadrature head coil [6]

2. METHODS AND MATERIALS

2.1 Anthropometric Analysis

According to Table 2.1, the mean values of neck circumference for each normal body mass index (BMI) male and female were 35.45 cm and 31.26 cm [7]. Table 2 shows the average of the midline and lateral neck length were 7.95 cm and 12.35 cm [8].

Table 2.1 Neck circumference among 18- to 20-year-old volunteers [7]

(Unit=cm)	Male (n = 41)	Female (n = 109)
Underweight (BMI < 18.5)	32.77 ± 1.68	30.29 ± 1.58
Normal (BMI 18.5- 22.9)	35.45 ± 1.23	31.26 ± 1.38
Overweight (BMI 23- 24.9)	36.20 ± 1.32	33.02 ± 0.98
Obese (BMI ≥ 25)	39.36 ± 2.56	33.89 ± 2.28

Table 2.2 Midline and lateral neck length of male and female [8]

(Unit=cm)	Midline Neck Length	Lateral Neck Length
Male	8.0	12.6
Female	7.9	12.1
Average	7.95	12.35

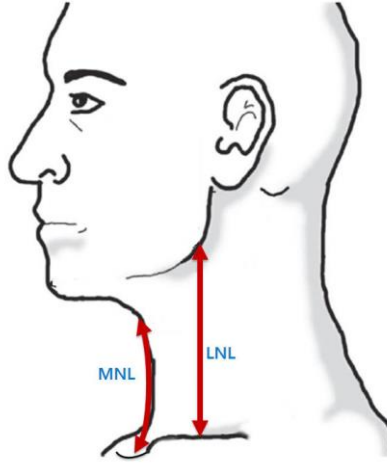


Figure 2.1 Reference line for neck length measurement. Midline neck length (MNL) was measured from the upper margin of the hyoid bone to the jugular notch. Lateral neck length (LNL) was measured from the mandibular angle to the mid-portion of the ipsilateral clavicle. [8]

2.2 Stretchable Fabric

2.2.1 MRI Scan

Ten different types of stretchable fabrics were scanned with GE 3.0T Discovery 750 to observe the effect of signal-to-noise ratio (SNR). Both T1 and T2 MR images were obtained while Vitamin E was located on the center of each fabric. The images were analyzed using the software MicroDicom. Table 2.3 was obtained by defining the center of fabric as the signal region of interest (ROI) and both side of the signal ROI as noise ROI. Figure 2.1 is included as an example of measurement. The collected value was calculated for SNR by Equation 2.1.

$$SNR = \frac{\text{Mean of Signal ROI}}{(\text{Std1} + \text{Std2})/2} \quad (2.1)$$

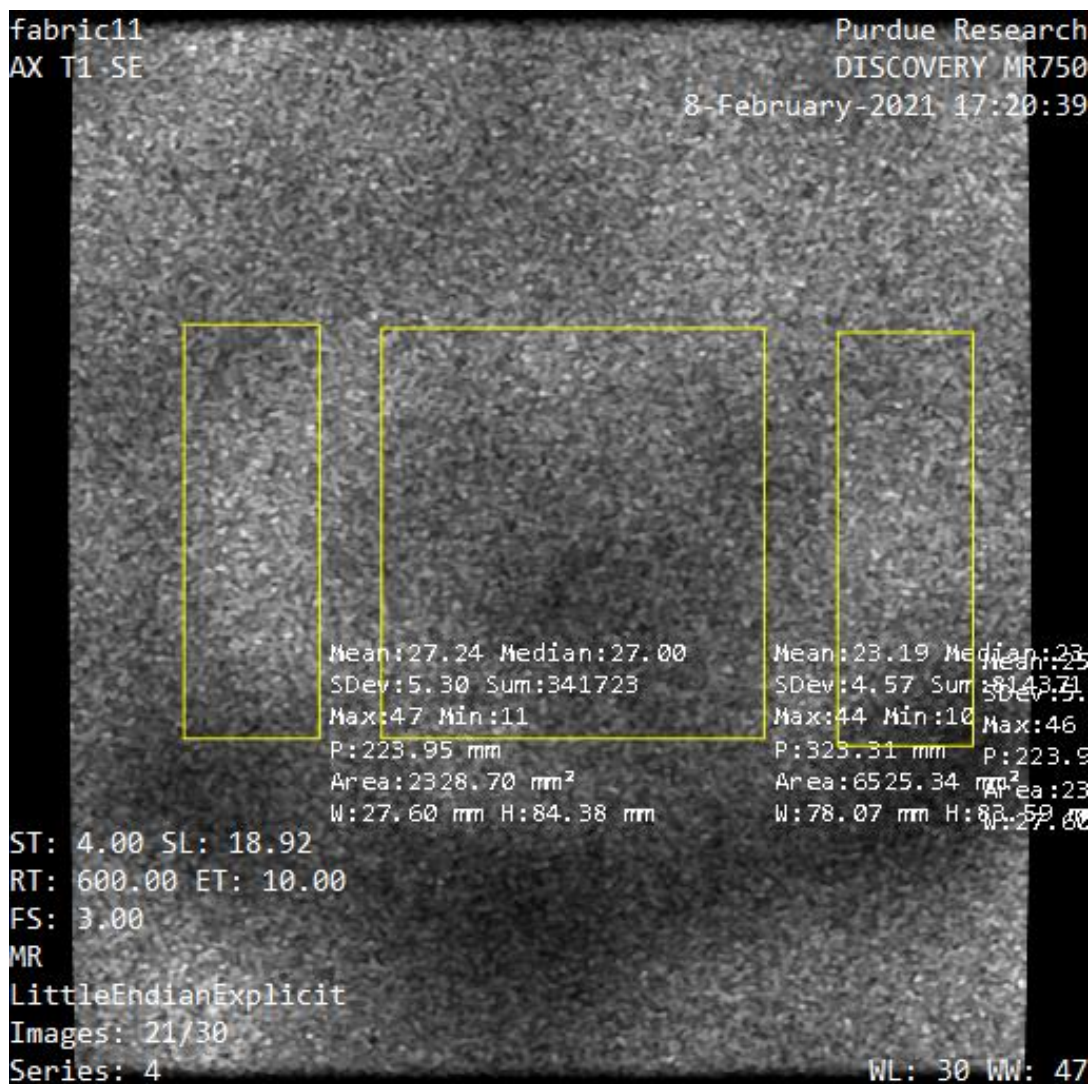


Figure 2.2 Example of signal ROI and noise ROI measurement

Table 2.3 Signal ROI and noise ROI values for 10 samples of stretchable fabrics

Scan	Content	Signal ROI	Noise ROI		SNR	
		Mean	Size (mm ²)	StD1		StD2
T1	87% 70/34 DL Nylon	24.810	2353.990	7.010	7.140	3.507
T2	13% 40 Denier Spandex	24.740	2360.200	4.880	5.250	4.885
T1	80% 70/24 SD Nylon	25.130	2357.870	8.050	7.340	3.266
T2	12% 15/1 SD Nylon	24.290	2351.630	5.440	4.620	4.829
	8% 40 Denier Spandex					
T1	64% 40/34 Dull Nylon	17.050	2357.870	3.830	4.850	3.929
T2	36% 54 Lycra	27.060	2355.870	5.230	4.410	5.614
T1	70% 40/34 Dull Nylon	21.800	2361.900	6.230	6.910	3.318
T2	30% 40 Lycra	24.090	2354.460	5.310	4.120	5.109
T1	81% 40/34 DL Nylon	26.550	2357.010	5.640	5.940	4.585
T2	19% 40 Denier Spandex	25.950	2357.880	4.700	4.570	5.599
T1	74% 40/24 Dull Recy. Poly	22.380	2354.250	4.850	4.690	4.692
T2	26% 55 Denier Spandex	22.380	2354.250	5.970	4.030	4.476
T1	87% 70/68 TXT Nylon	23.900	2355.550	7.190	7.350	3.287
T2	13% 210 Denier Spandex	28.750	2357.240	5.820	4.780	5.425
T1	88% 70/72 SD TXT Polyester	25.670	2355.910	6.550	9.590	3.181
T2	12% 40 Denier Spandex	27.660	2356.860	4.820	3.770	6.440
T1	81% 70/34 DL Nylon	23.980	2355.550	6.310	6.900	3.631
T2	19% 280 Denier Spandex	25.750	2354.250	4.770	3.250	6.421
T1	64% 70/34 Nylon	25.460	2353.720	5.880	7.820	3.717
T2	29% 40/13 DL Nylon	27.890	2357.880	5.310	3.600	6.260
	7% 40 Denier Spandex					

2.2.2 Embroidery and Design

Thickness of the chosen conductive thread exceeded the maximum bobbin and spool thread size for the embroidery machine (VE2200, Brother). Therefore, the preset zigzag pattern of the embroidery machine was performed with regular thread on the stretchable fabric to outline the uniform stitch pattern, and the spool thread was pulled out to insert the conductive thread along with the stitch.

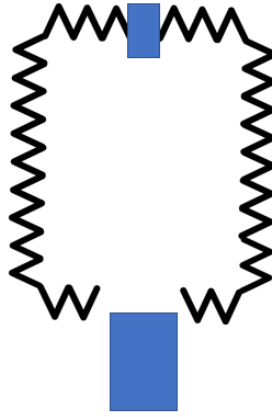


Figure 2.3 Outline of stitch pattern with hook-and-loop anchors

Moreover, a piece of hook-and-loop fastener (Velcro) was attached to anchor the matching and tuning board, and the tuning capacitor on the middle of the conductive thread as shown in Figure 2.3. The top blue rectangle was designed for the tuning capacitor, and the bottom blue rectangle was for the matching and tuning board. These anchors support the components of the RF coil and prevent them from expanding when the coil is stretched.

2.3 Conductive Thread

2.3.1 Impedance Measurement

The impedance of LYO337Cu (Syscom Advanced Materials, Inc.) and LYO332Ag (Syscom Advanced Materials, Inc.) were measured on the plastic bench using the network analyzer (E5071C, Keysight Technologies) connected with the multiport test set (E5091A, Agilent Technologies). LYO337Cu is made of 80% copper, and LYO332Ag is made of 80% silver. Both have 4.5 twists per inch and dc resistance of $1\ \Omega$ per foot.

Oval and circle shaped frames were used to measure impedance of each thread on the plastic bench. The 10.5-cm width and 22.5-cm height of the oval frame was wrapped with 64 cm of thread, and the 12.5-cm diameter circle frame was wrapped with 50 cm of thread (Figure 2.4). The end of each thread was connected to the BNC connector to measure impedance using the network analyzer, with a measurement span of 120-300 MHz.



Figure 2.4 Oval (left) and circle (right) frames used for the impedance measurements

Table 2.4 Impedance of oval shaped and circle shaped frame in $R+jX$ form on Smith chart

	Oval Shaped Frame		Circle Shaped Frame	
	R (Ω)	X (Ω)	R (Ω)	X (Ω)
LYO332Ag	1.3501k	-1.3119k	962.41	-1.3146k
	70.414	-293.48	83.930	-293.09
LYO337Cu	1.5032k	-1.3186k	1.2998k	-1.3033k
	58.352	-294.08	406.34	-294.23

2.4 Tuning and Matching Board

2.4.1 Printed Circuit Board Layout

Printed circuit board (PCB) was designed with EAGLE software (Autodesk, Inc.) and exported to LPKF to mill the top copper layer (Figure 2.5). The board was placed on heated plate to remove the excess copper from the top layer according to the layout, creating the final board (Figure 2.6).

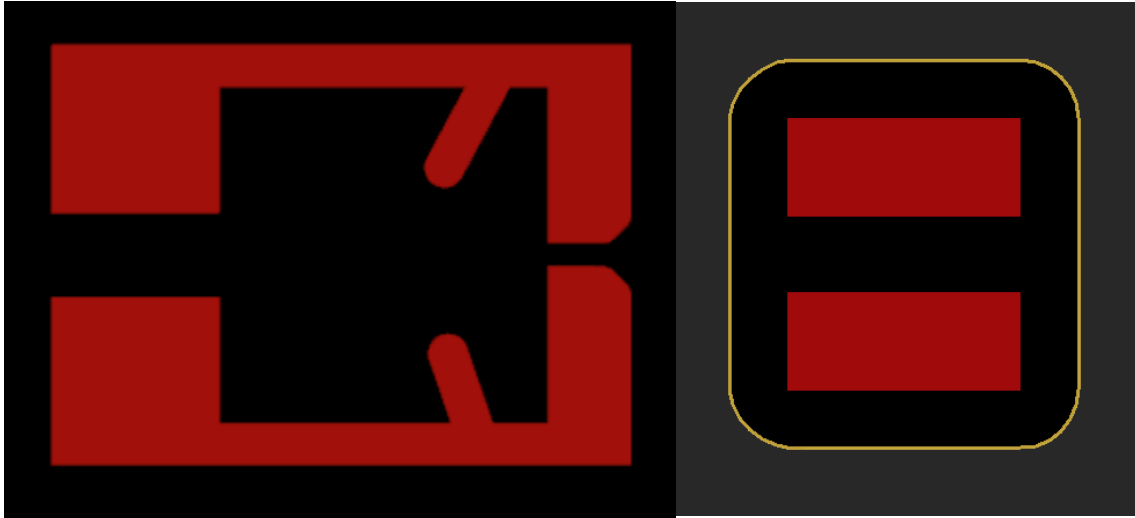


Figure 2.5 Example PCB board layouts in EAGLE software



Figure 2.6 Sample printed PCB board

2.4.2 Balun

A 3T balun was placed between two probes for tuning on S_{21} measurement (Figure 2.7). Capacitor adjustment sticks were attached on the balun to tune the peak to 128 MHz (Figure 2.8). The balun was soldered to connect the PCB board to the coaxial cable with the BNC connector.



Figure 2.7 Bench setup of the S_{21} measurement for tuning a balun

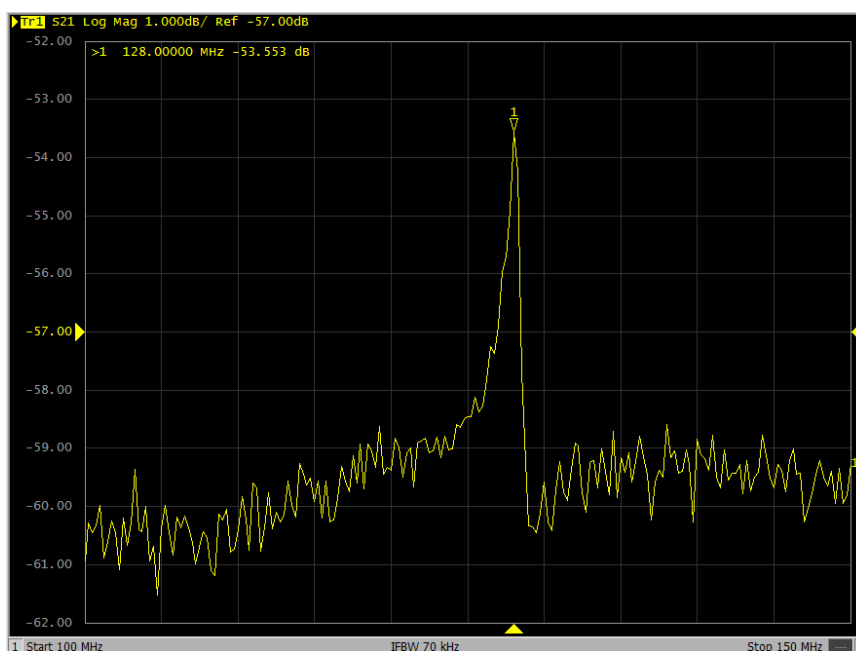


Figure 2.8 Example S_{21} measurement of the balun with 27-pF capacitor

2.4.3 Bench Measurement

The S_{11} and S_{21} measurements were performed on the plastic bench for each single channel. While testing a channel, other channels were closed with a piece of copper tape. The RF coil with coaxial cable was connected to the network analyzer with a ferrite toroid for both S_{11} and S_{21} measurements.

Each stretchable neck RF coil element was soldered with the tuning and matching board as diagrammed in Figure 2.9 for tuning to 128 MHz. The S_{11} measurement was performed by connecting the RF coil element to the network analyzer to find a dip at 128 MHz. The S_{21} measurement was performed by connecting port 1 of the network analyzer to the RF coil element and port 2 to the single-loop probe. The probe was placed 2 cm above the center of the stretchable coil (Figure 2.10). The quality factor was calculated by the network analyzer based on the S_{21} measurement.

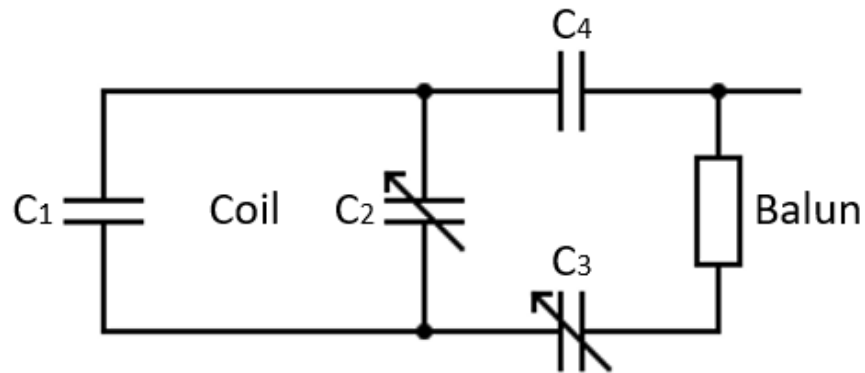


Figure 2.9 Schematic of the RF coil connected to the tuning and matching capacitors only. C_1 and C_2 are matching capacitors, and C_3 and C_4 are tuning capacitors. C_2 and C_3 are variable capacitors to adjust capacitance. C_3 and C_4 have equal capacitance.

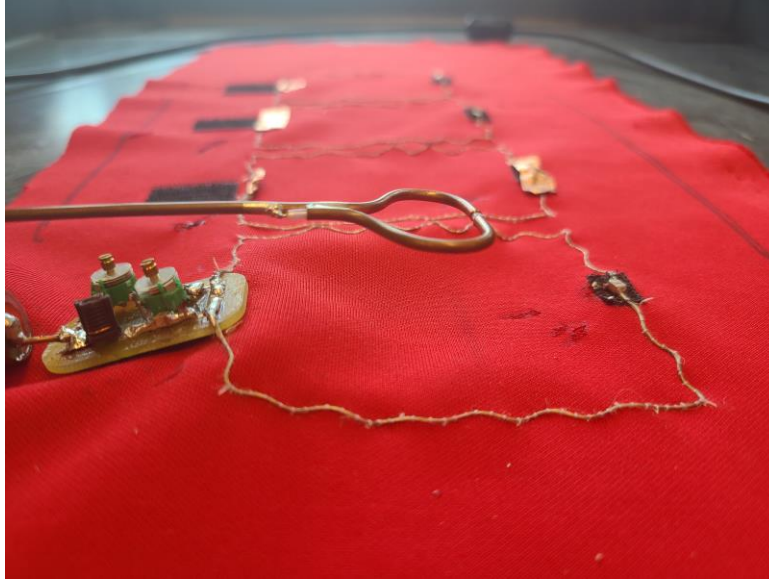


Figure 2.10 S_{21} measurement with coil, as indicated in Figure 2.9, and single-loop probe

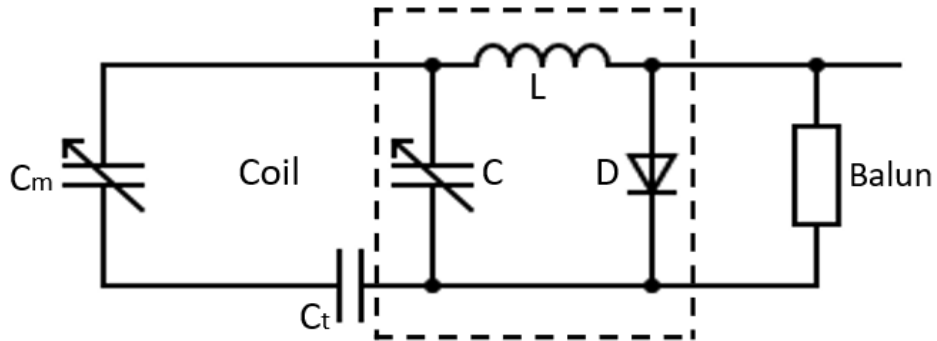


Figure 2.11 Schematic of the RF coil connected to the final tuning and matching board including inductor and diode. C_m is for matching and C_t is for tuning. The dashed region is the trap comprised of L , C , and D .

Each RF coil element was connected to a final tuning and matching board as diagrammed in Figure 2.11 to measure the active detuning. Prior to the measurement of tuned and detuned states, the active detuning trap was tuned using a solenoid sniffer probe. C_m was removed to create an open circuit. To switch on the forward-biased PIN diode, the dc power supply was connected to a series 10- Ω resistor to apply 5-V bias. Referring to Figures 2.12 and 2.13, the trap was tuned at 128 MHz [9].

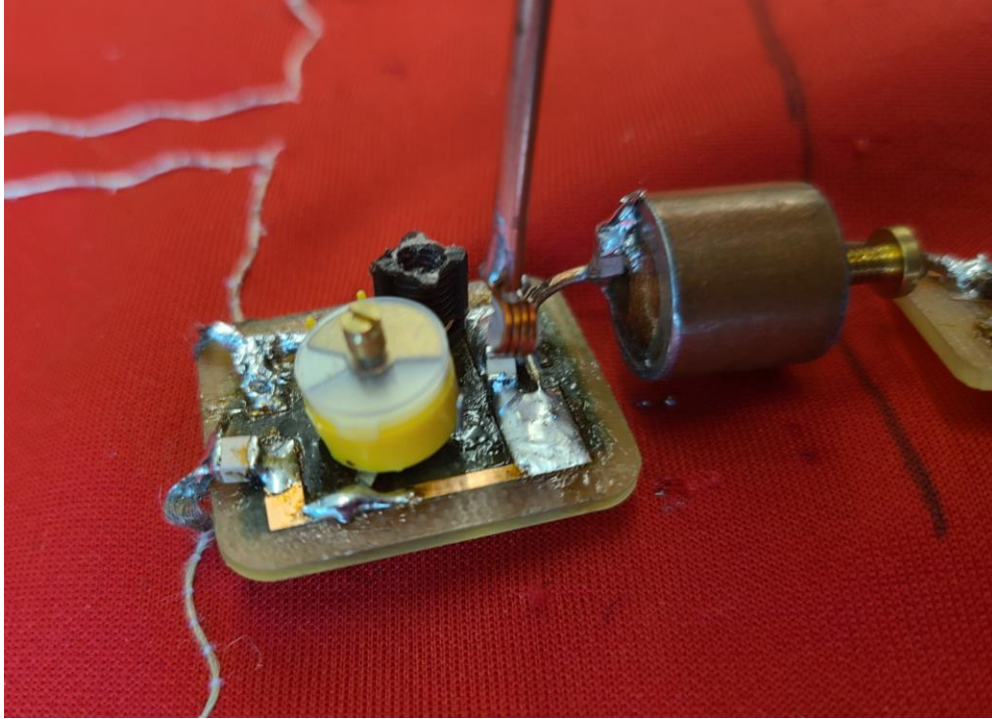


Figure 2.12 Pre-adjustment of the active detuning trap using a sniffer probe

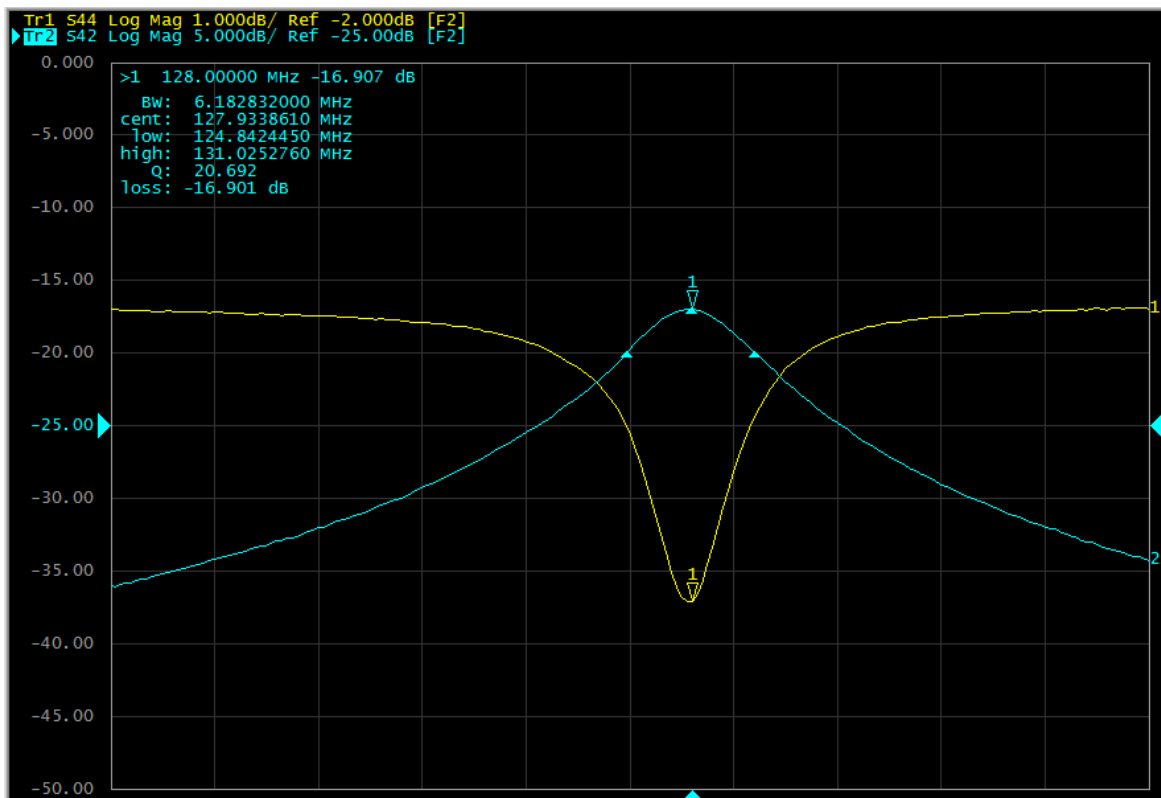


Figure 2.13 S_{11} (yellow) and S_{21} (cyan) measurements of the active detuning trap

After tuning the trap, C_m was attached back to its position to make a closed loop. Then, the S_{21} measurement was performed to tune the coil loop at 128 MHz with and without the forward bias of 5V and 0.4A, which was connected with 10- Ω resistor in series. During the measurement, a 50- Ω load was connected to the coil cable, as it was not connected to the network analyzer. An overlapped double-loop probe was placed 2 cm above the center of the loop for the S_{21} measurement. The procedure was repeated on each channel on the plastic bench and while wrapped around the dielectric muscle phantom. The peak of the tuned state (diode off) and dip of the detuned state (diode on) was compared.



Figure 2.14 S_{21} measurement with an overlapped double-loop probe on a dielectric muscle phantom

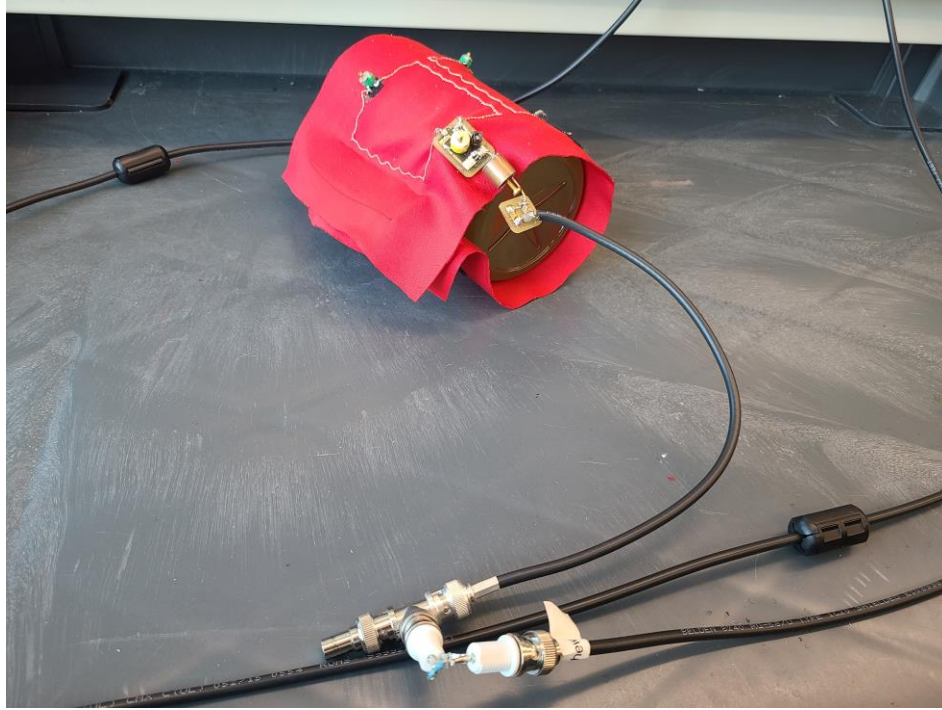


Figure 2.15 Setup of the S_{21} measurement loaded with the muscle phantom

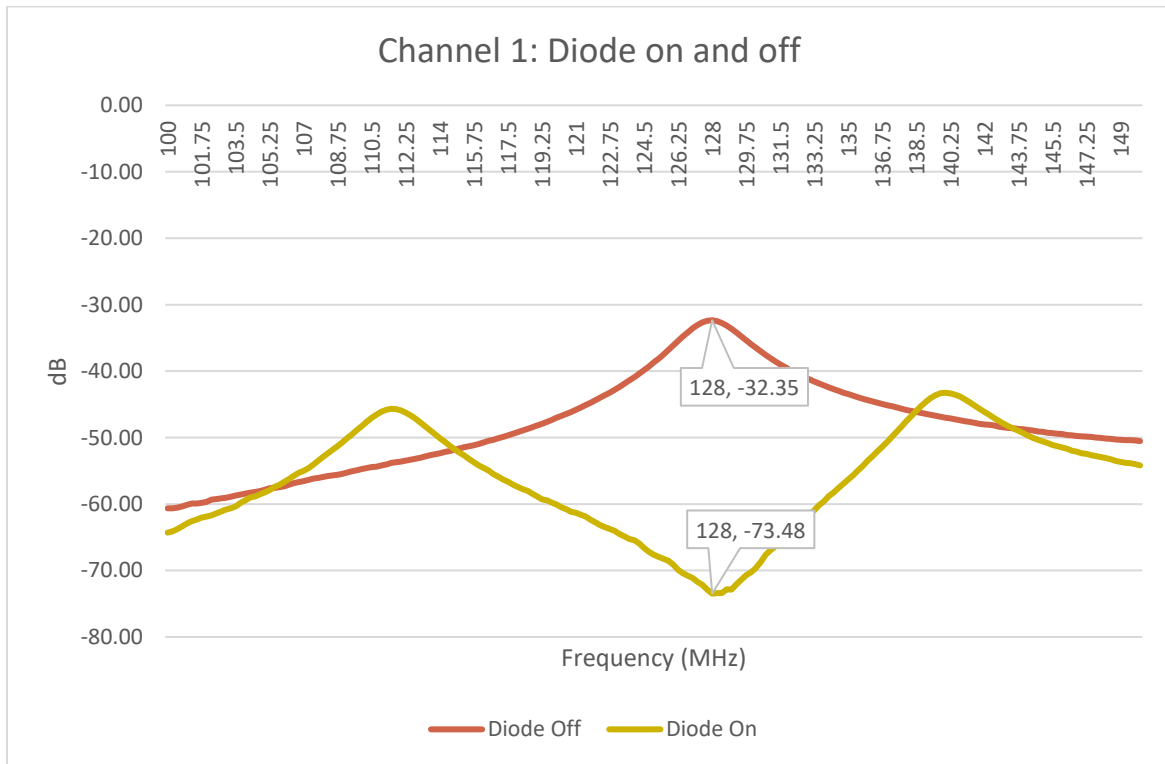


Figure 2.16 S_{21} measurement of the tuned state (diode off) and dip of the detuned state (diode on) of channel 1 on the plastic bench.

2.4.4 Quality Factor

The quality factor (Q-factor) is a unitless parameter to measure the ratio of the stored and dissipated energy at the resonant frequency [10]. Higher Q-factor indicates lower loss and better performance of the RF coil. The f_0 and f_{3dB} of each channel were collected using S_{21} measurements on the plastic bench. The network analyzer automatically detects f_0 and f_{3dB} and calculates the Q-factor (Figure 2.17). The stretchable coil was measured on an empty plastic cylinder for the unloaded Q-factor and on the dielectric phantom for the loaded Q-factor.

$$Q = \frac{f_0}{f_{3dB}} \quad (2.2)$$

$$Q_{ratio} = \frac{Q_{unloaded}}{Q_{loaded}} = \frac{R_{Coil} + R_{Sample}}{R_{Coil}} \quad (2.3)$$

Equation 2.2 shows how Q-factors were calculated by the network analyzer. The ratio of Q-factors of the unloaded and loaded states (Equation 2.3) indicates the coil sensitivity within the sample. Large R_{sample} compared to R_{coil} indicates a good circuit design, as the Q_{ratio} greater than 2 is referred to as sample noise dominance [5].

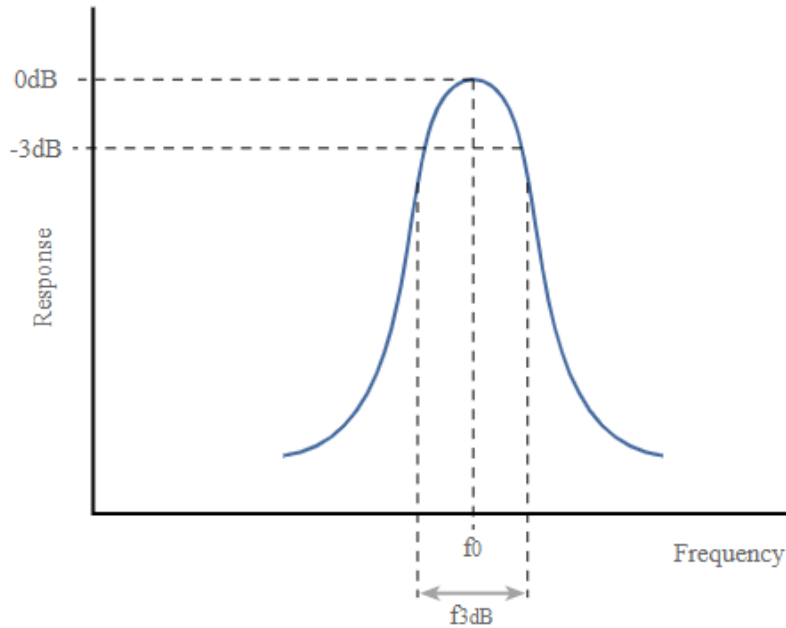


Figure 2.17 Q-factor showing the peak and -3dB points [11]

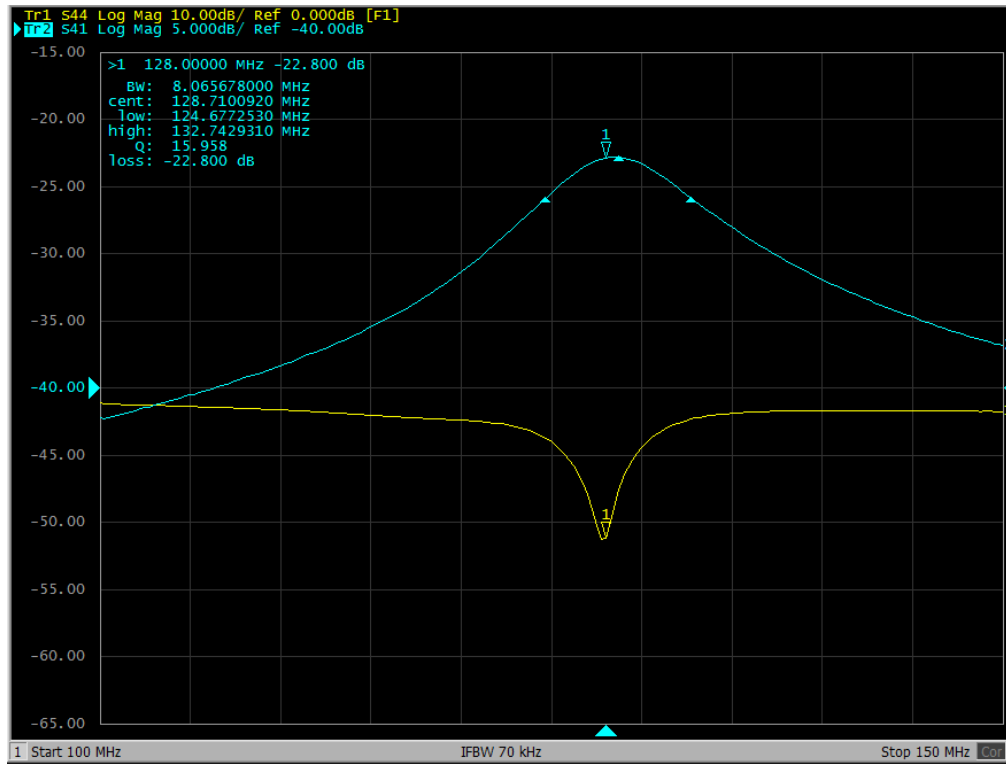


Figure 2.18 Example automated Q-factor measurement on the network analyzer

2.5 Dielectric Phantom

2.5.1 Dielectric Phantom Recipe

Muscle has the characteristics of 63.5 relative permittivity and 0.719 S/m conductivity at 128 MHz [12]. Referring to the information, the dielectric phantom recipe was designed using the dielectric phantom recipe generator from the National Institutes of Health [13]. Sucrose ingredients were used to match the desired gel characteristics.

According to the dielectric phantom recipe generator, 700 mL of water, 23.29 g of NaCl, 637.24 g of sugar, 10.5 g of 1.5% agar, and 0.7 g of 0.1% of benzoic acid were required [12]. However, using the Dielectric Assessment Kit (DAK, SPEAG), the resulting measured permittivity was high and the conductivity was low compared to the desired characteristics. To match with the relative permittivity of 63.5 and conductivity of 0.719 S/m, an additional 320 g of sugar and 10 g of NaCl were added.

Moreover, 0.7 g of copper sulfate (CuSO_4) was added to affect the proton relaxation characteristics for MRI [14]. Using a cylindrical plastic container of 30-cm circumference and 15.3-cm height (including the lid), the phantom was sealed with masking tape (Figure 2.19).

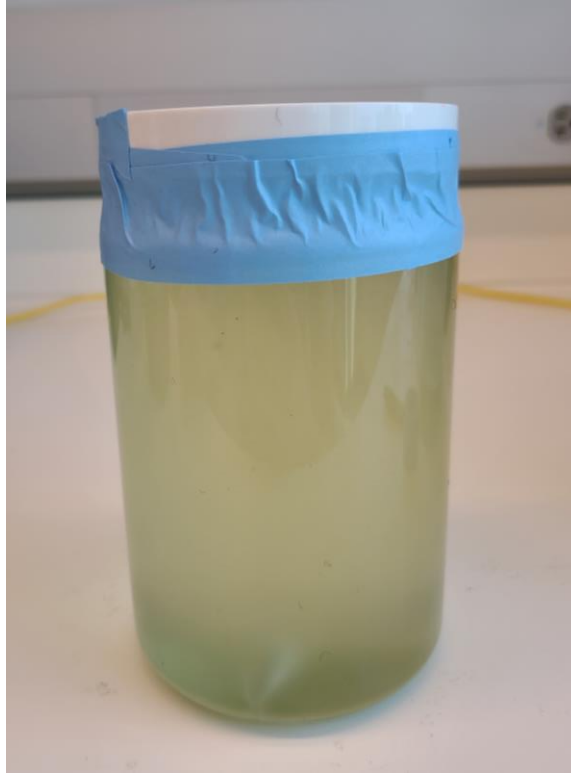


Figure 2.19 Photograph of cylindrical muscle-mimicking dielectric phantom

2.5.2 DAKS Measurement

The DAK-12 (SPEAG) was attached to the R60 Vector Reflectometer (Copper Mountain Technologies) to measure the permittivity and the conductivity of the dielectric phantom. For the calibration, the Open-Short-Load (OSL) method was used. The open circuit measurement was performed by leaving the probe in air [15]. The probe tip was wiped with isopropyl alcohol and allowed to dry for one minute. The short circuit measurement was performed by placing a copper strip on the shorting block. The copper strip was rubbed with a fine piece of sandpaper and wiped with isopropyl alcohol before use. The load measurement was performed by placing the probe in a beaker of distilled water.

The permittivity and conductivity of the dielectric phantom were measured using DAKS after the calibration. Data were collected from 100-150 MHz to determine the characteristics of phantom at 128MHz.

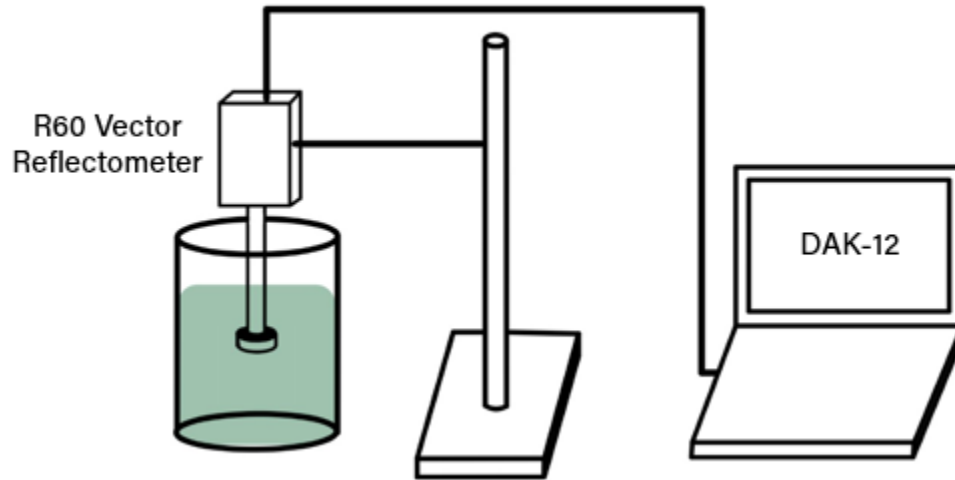


Figure 2.20 Process of DAKS measurements. The DAK-12 (SPEAG) was attached with R60 Vector Reflectometer (Copper Mountain Technologies) to measure the permittivity and the conductivity of the dielectric phantom.

2.6 MRI Scan

2.6.1 Method

T1 and T2 weighted MRI scans were performed by wrapping the phantom with the stretchable 4-channel RF coil on GE 3.0T Discovery 750. For the T1 scans, axial and IDEAL sequences were performed. IDEAL is a sequence allowing four contrast types with one scan: water only, fat only, in-phase, and out-of-phase. It produces scanned images as shown in Figure 2.21. Axial and sagittal slices were chosen to analyze the RF coil in diverse planes.

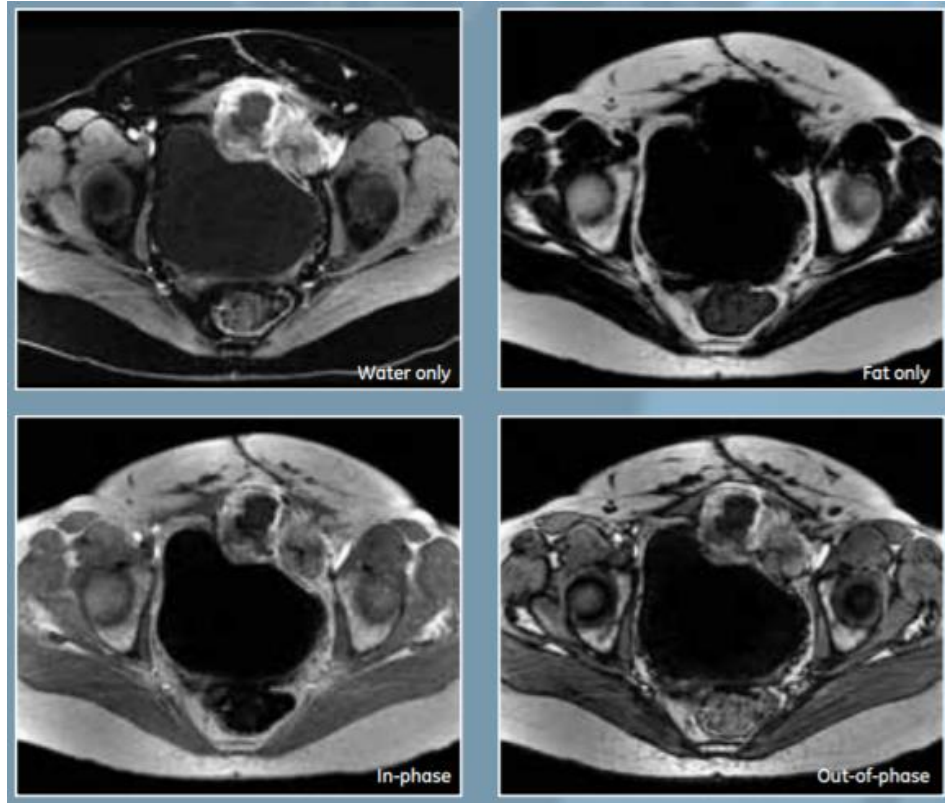


Figure 2.21 Abdominal image scanned with IDEAL sequence [16]

The SNR of the scanned images were calculated using Equation 2.1. A 7×7 -pixel region of signal and an 11×11 -pixel region of noise were selected on the software microDicom. The average of the standard deviations of the four regions marked in yellow (Figure 2.22) was calculated as noise signal, and three different signal regions were designated to calculate the SNR of each location in the axial T1-weighted image. The SNR of the dielectric phantom on the scanned images is expected to be lower in the middle of the phantom compared to the surface near the coil. The SNR calculation for the sagittal T2-weighted image on the center and the surface of the phantom was also demonstrated by designating the two yellow regions as noise signal, as shown in Figure 2.23.

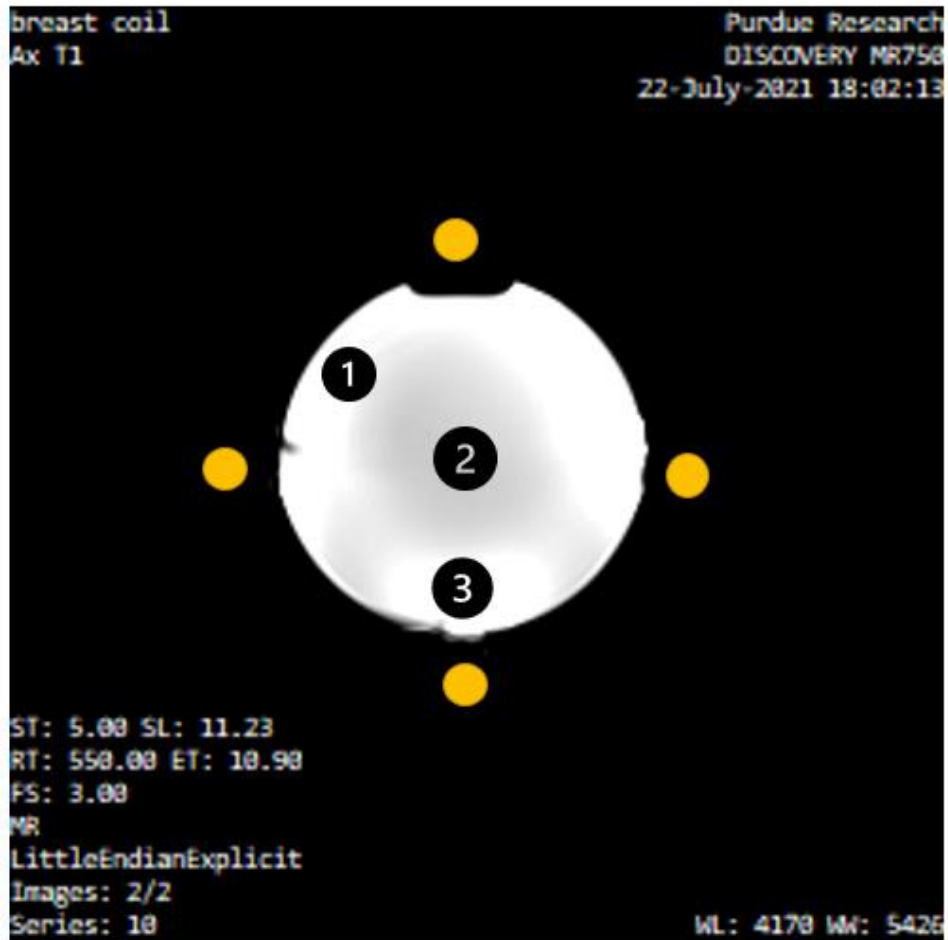


Figure 2.22 Regions of noise (yellow) and regions of signal (numbered) used for the SNR calculation in the axial T1 image. Signal region 1 is the gap between the coil near the surface of the phantom, 2 is the center of the phantom, 3 is the center of coil near the surface of the phantom.



Figure 2.23 Regions of noise (yellow) and regions of signal (numbered) used for the SNR calculation in the sagittal T2 image. Signal region 1 is the center of the phantom, 2 is the center of the coil near the surface of the phantom.

3. RESULTS

3.1 Stretchable Coil

3.1.1 Specifications of the Coil

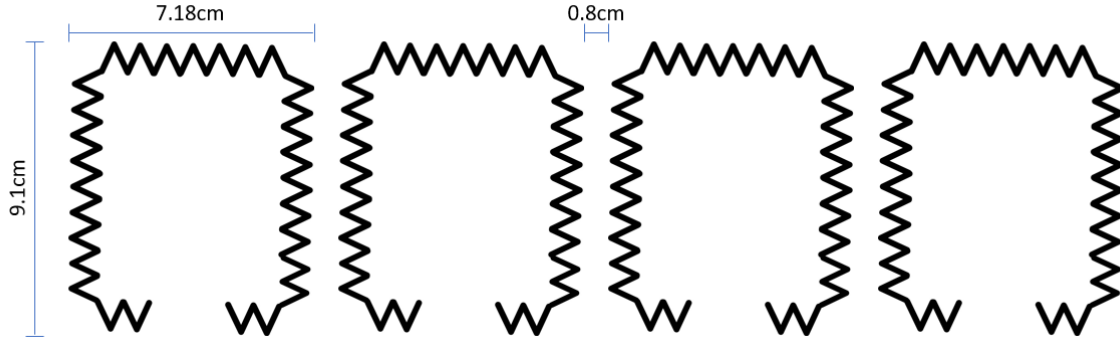


Figure 3.1 Zigzag stitch pattern dimensions

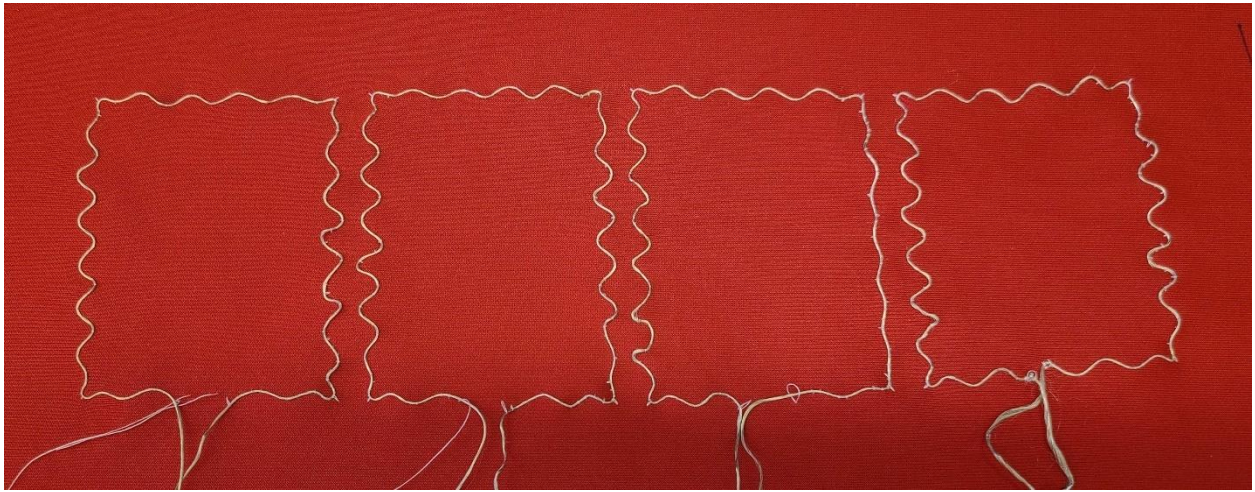


Figure 3.2 LYO332Ag stitched on the stretchable fabric in zigzag pattern

Considering the average neck circumference, midline, and lateral neck length, as detailed in section 2.1, each RF coil element was designed in zigzag pattern in rectangle of 7.18-cm width and 9.1-cm height. The total size of the flat neck RF coil is 32-cm width and 13-cm height. Hook-and-loop fastener was attached at two ends of the coil for the measurements on the phantom.

Table 2.3 showed that fabric materials have minimal effects on the quality of the MR image. Table 2.4 also depicted that the measured impedance of LYO332Ag was more efficient as it has lower resistance than LYO337Cu. Therefore, LYO332Ag was stitched on the fabric composed of 94% polyester and 6% spandex with the preset zigzag pattern of the embroidery machine. In addition, a piece of hook-and-loop fastener (Velcro) was attached on the top of the stretchable coil to fix the tuning capacitor.

3.2 Bench Measurements

3.2.1 Balun

A 3T balun was tuned by placing capacitor adjustment sticks to determine the required capacitance, as shown in Figures 2.7 and 2.8. A 27-pF ceramic capacitor was soldered on a balun to tune at 128 MHz. Then, a coaxial cable was attached to the balun on the connection PCB.

3.2.2 Dielectric Muscle Phantom Analysis

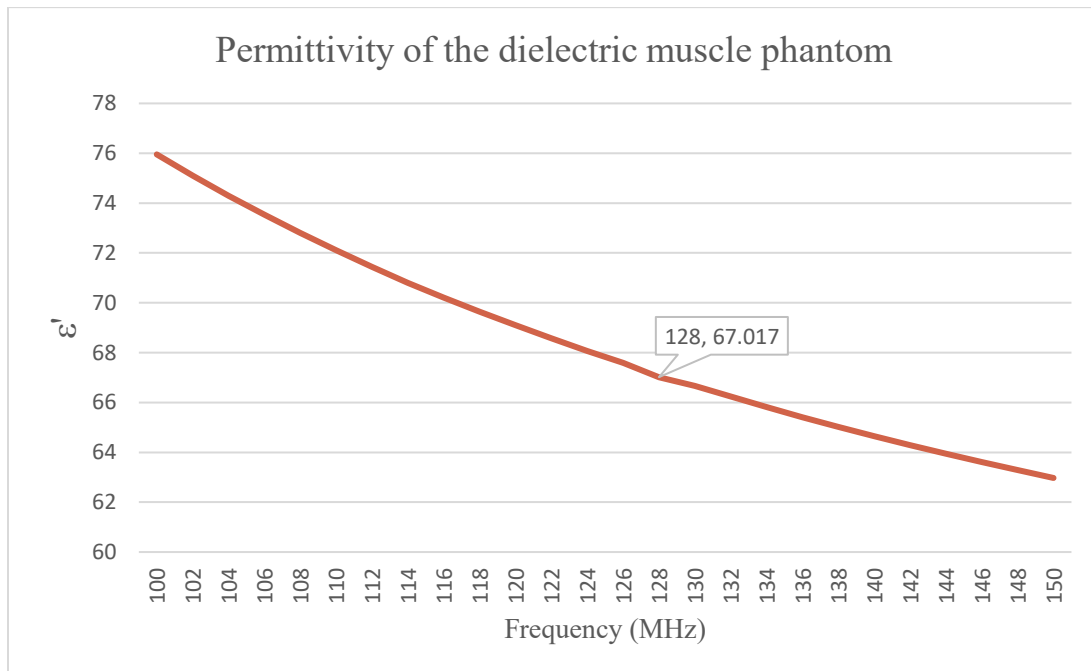


Figure 3.3 Relative permittivity of the dielectric muscle phantom measured using DAKS

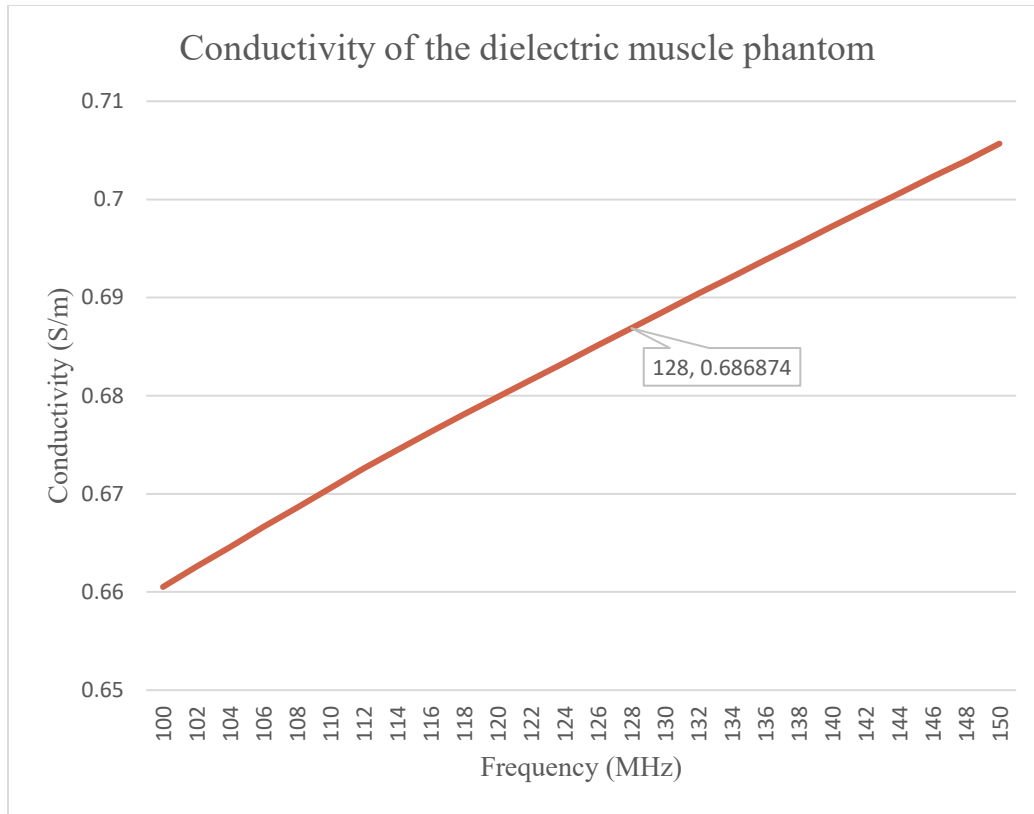


Figure 3.4 Conductivity of the dielectric muscle phantom measured using DAKS

The calculated percent error of the permittivity and conductivity were 5.70% and 4.47%, as detailed in Table 3.1. Considering the characteristics of liquid phantoms, the percent error is acceptable because it is not completely homogeneous, and the components are constantly moving within the liquid. Both permittivity and conductivity changed constantly when stirring. Therefore, the value was recorded 10 minutes after stirring.

Table 3.1 Theoretical and experimental values of relative permittivity and conductivity of the dielectric muscle phantom with the calculated percent error

	f (MHz)	ϵ'	σ (S/m)
Theoretical Value	128	63.50	0.719
Experimental Value	128	67.12	0.687
Percent Error (%)		5.70	4.47

3.2.3 Coil Testing

For the final bench measurements on the phantom and the MRI scans, the matching capacitor on Figure 2.11 was adjusted to tune at 128 MHz, first while on the plastic bench, and finally while the coil was wrapped around the dielectric phantom. The matching capacitor was the only component that required slight adjustment, because the graph was left skewed approximately 1.5 MHz when measured on the phantom compared to on the plastic bench. Active detuning performance is detailed in Tables 3.2-3.3 and illustrated in Figures 3.5-3.8. Quality factors are listed in Table 3.4 with example measurement plots shown in Figures 3.9-3.10.

Table 3.2 S_{21} measurement of the coil on the plastic bench with and without 5-V forward bias applied to the PIN diode trap

Channel	Diode off (dB)	Diode on (dB)	Difference (dB)
1	-32.35	-73.48	41.13
2	-35.48	-70.48	35.00
3	-33.00	-70.69	37.69
4	-33.82	-71.05	37.23

Table 3.3 S_{21} measurement of the coil on the dielectric phantom with and without 5-V forward bias applied to the PIN diode trap

Channel	Diode off (dB)	Diode on (dB)	Difference (dB)
1	-37.87	-72.89	35.02
2	-38.69	-70.47	31.79
3	-38.19	-69.81	31.62
4	-37.39	-70.47	33.09

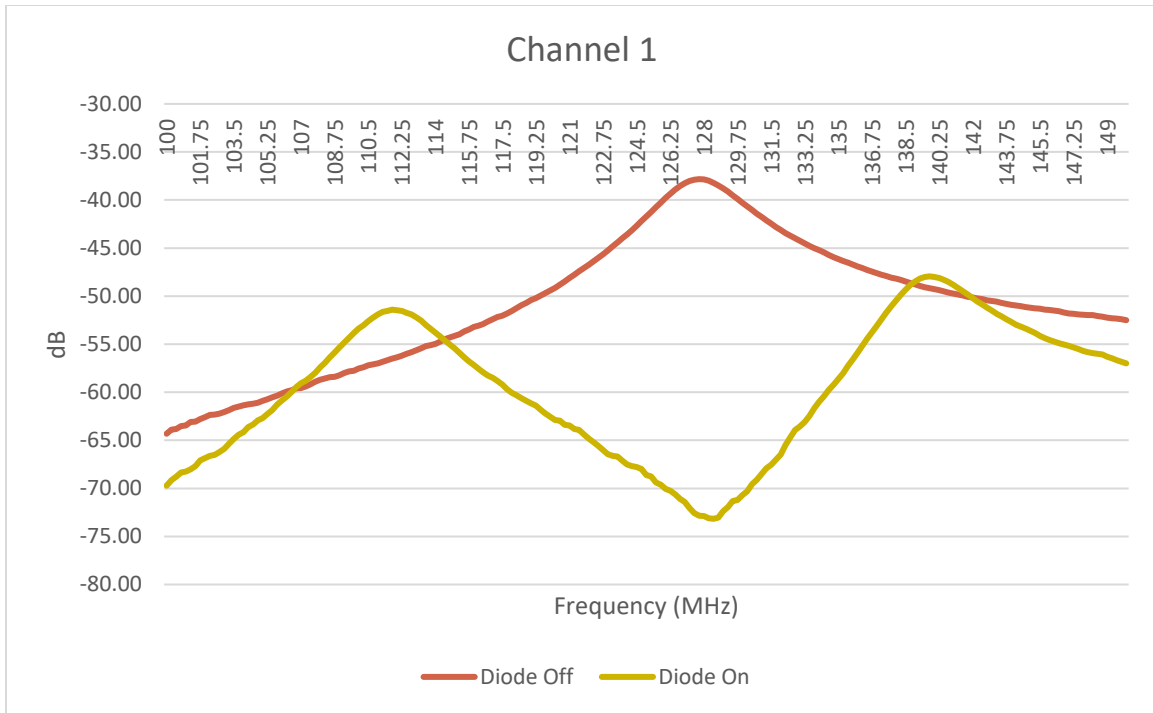


Figure 3.5 S_{21} measurement of the coil on the dielectric phantom with and without 5-V forward bias applied to the PIN diode trap for the channel 1

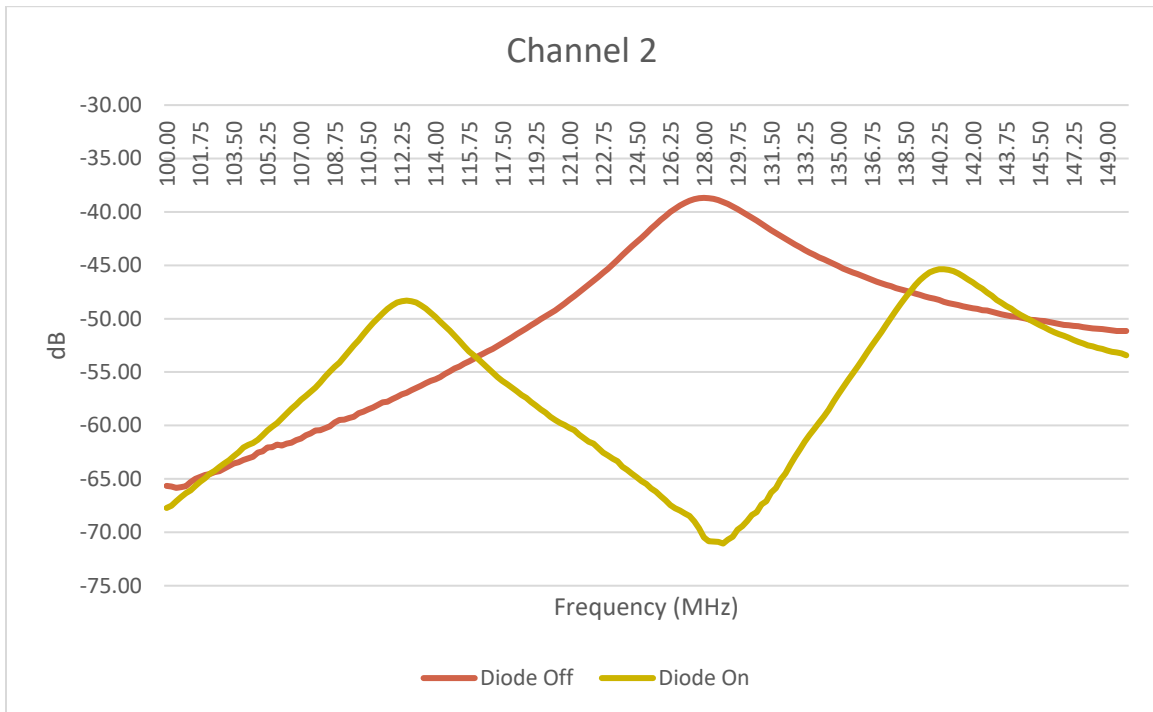


Figure 3.6 S_{21} measurement of the coil on the dielectric phantom with and without 5-V forward bias applied to the PIN diode trap for the channel 2

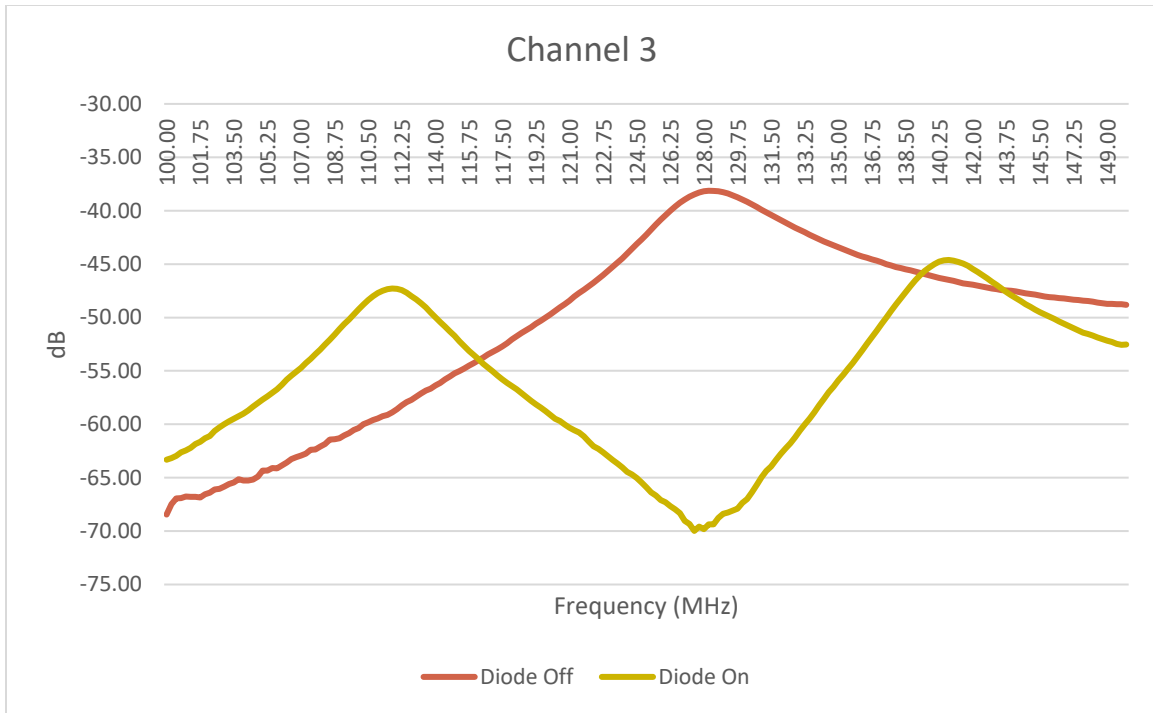


Figure 3.7 S_{21} measurement of the coil on the dielectric phantom with and without 5-V forward bias applied to the PIN diode trap for the channel 3

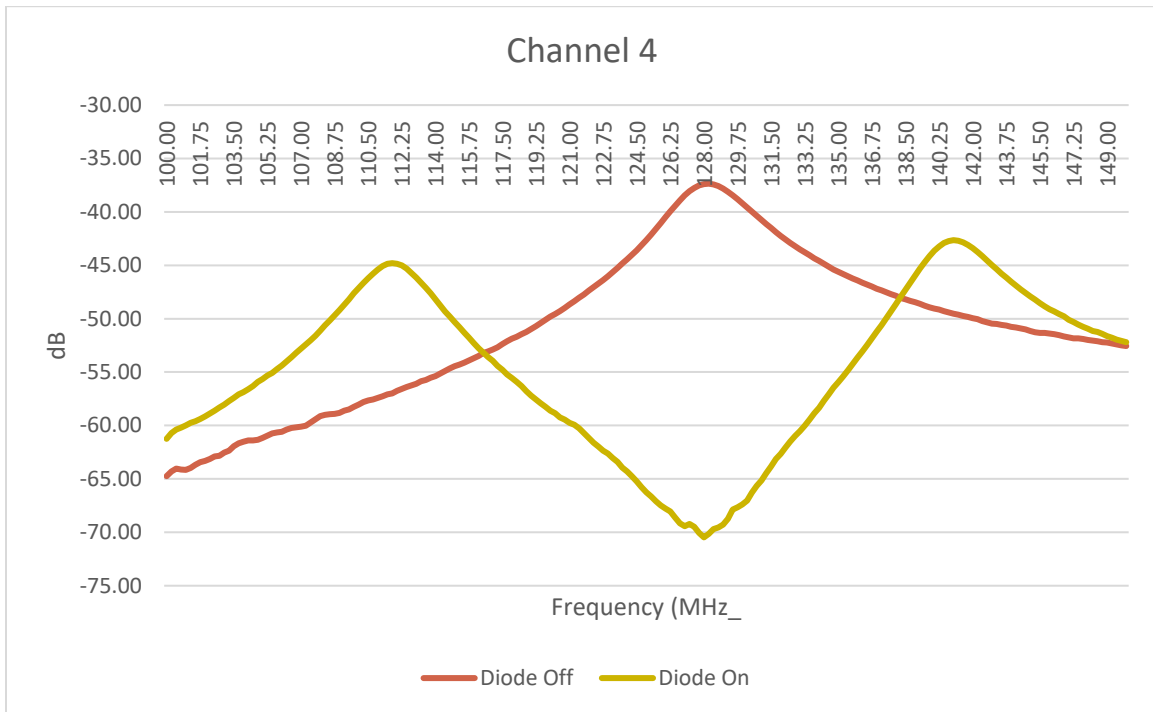


Figure 3.8 S_{21} measurement of the coil on the dielectric phantom with and without 5-V forward bias applied to the PIN diode trap for the channel 4

Table 3.4 Quality factors from the unloaded and loaded measurements. Ratio refers to the unloaded to the loaded.

Channel	Unloaded	Loaded	Ratio
1	30.134	15.182	1.985
2	32.791	15.779	2.078
3	31.292	15.067	2.077
4	32.028	15.958	2.007

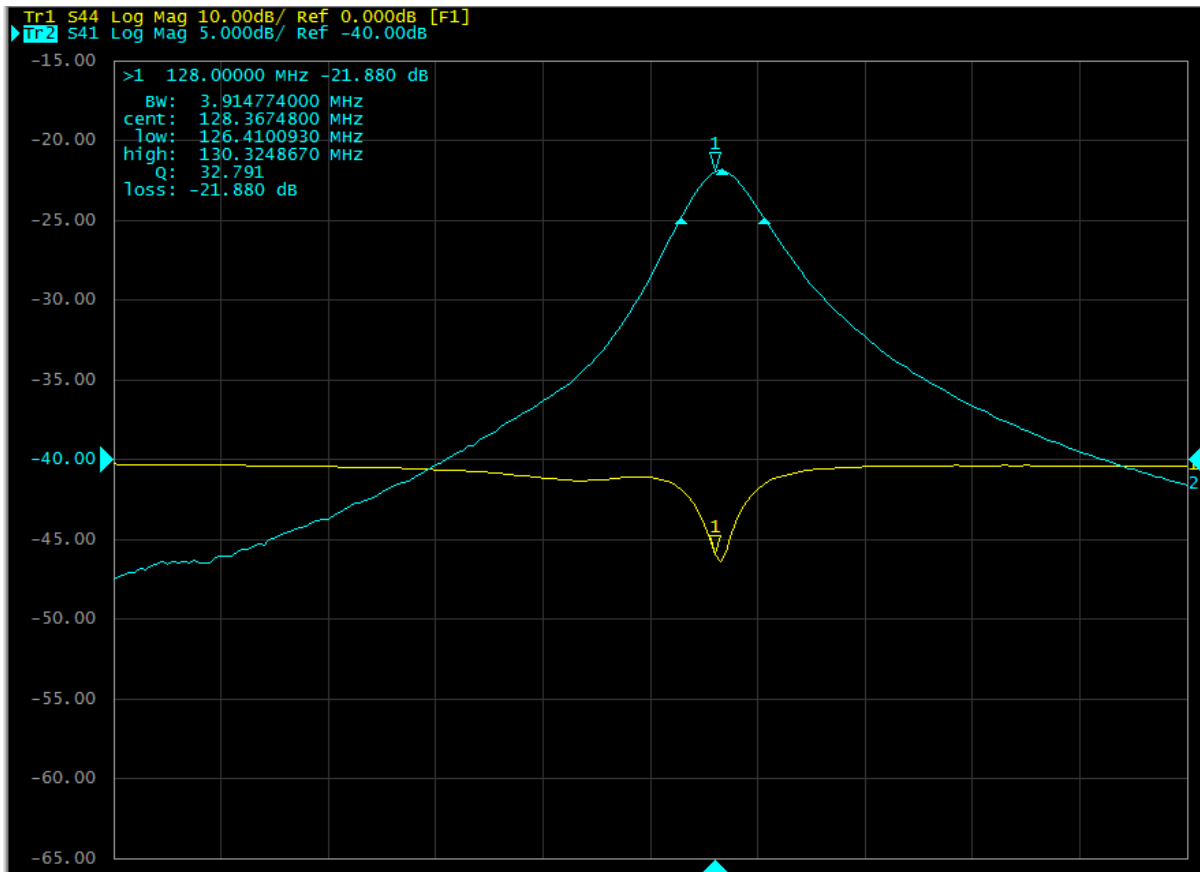


Figure 3.9 Q-factor measurement of the channel 2 on the plastic bench

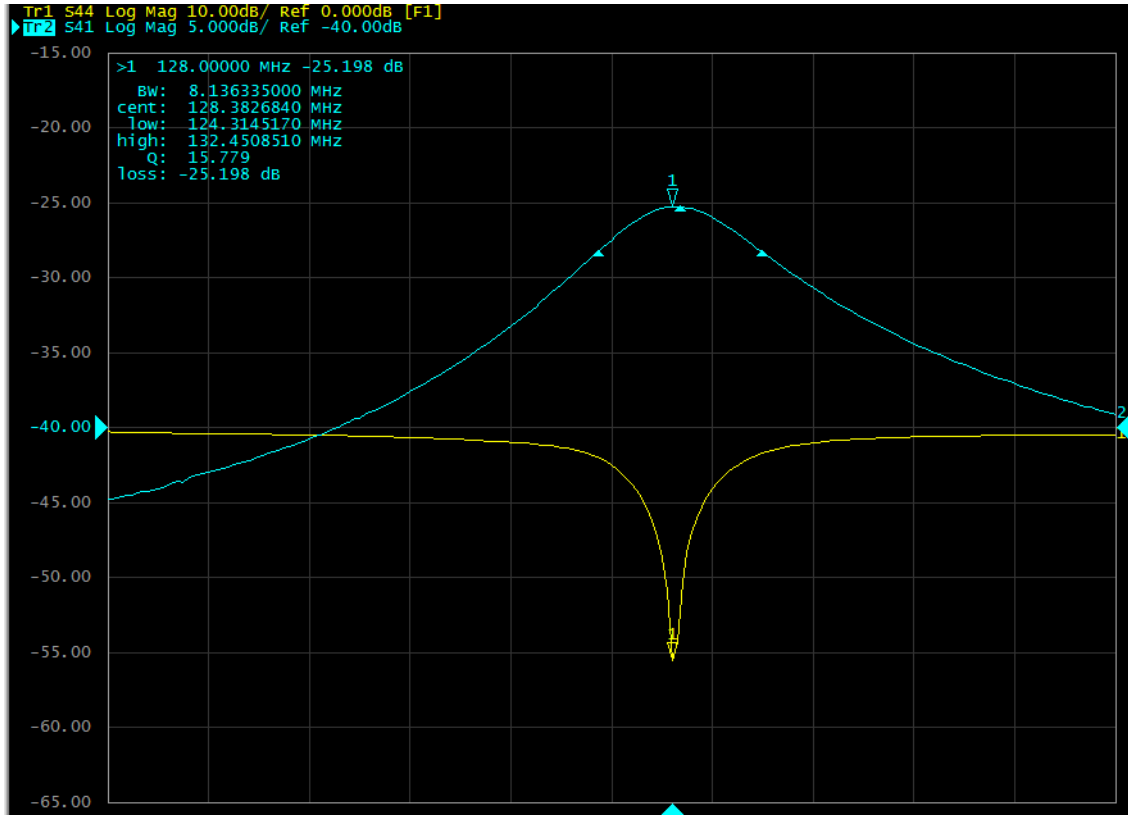


Figure 3.10 Q-factor measurement of the channel 2 on the dielectric phantom

3.3 MRI Analysis

3.3.1 Dielectric Phantom Scan

The dielectric phantom was scanned for axial T1, IDEAL T1, and sagittal T2. Brightness and windowing were adjusted to accentuate the brightness near the coil. The small shaded regions between the coil channels were observed on the scanned images due to the close proximity of the conductor stitch. However, this effect would be able to be adjusted by placing a thin spacer between the neck and the coil to acquire the image as it only affects less than 0.5-cm deep from the surface of the phantom while the range of the average thickness of adult neck skin is $3946 \pm 109.158 \mu\text{m}$ for lateral neck and $4294 \pm 69.314 \mu\text{m}$ for ventral neck [17].

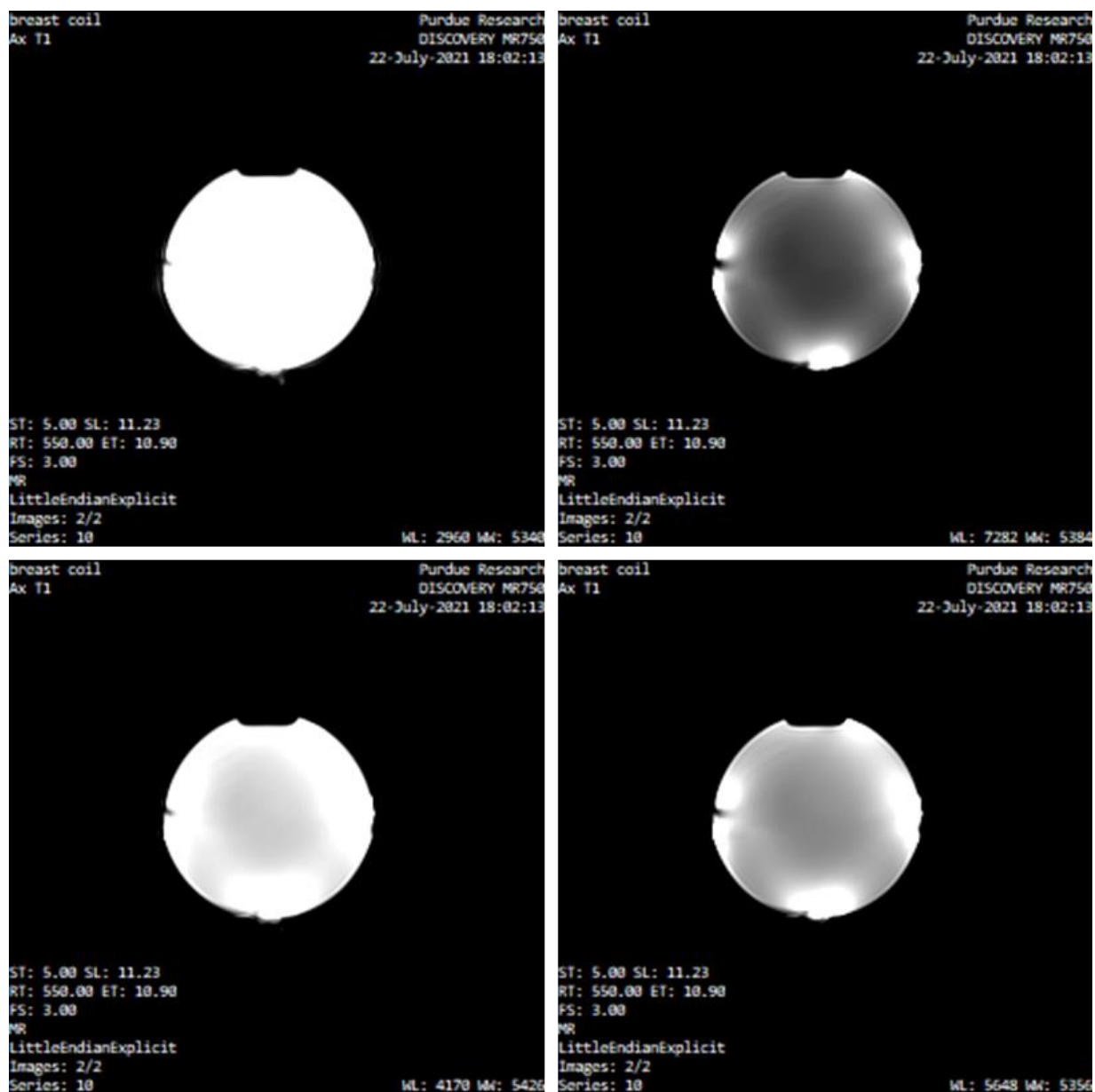


Figure 3.11 Axial T1-weighted MRI scan. Brightness and windowing were adjusted to accentuate the brightness near the coil.

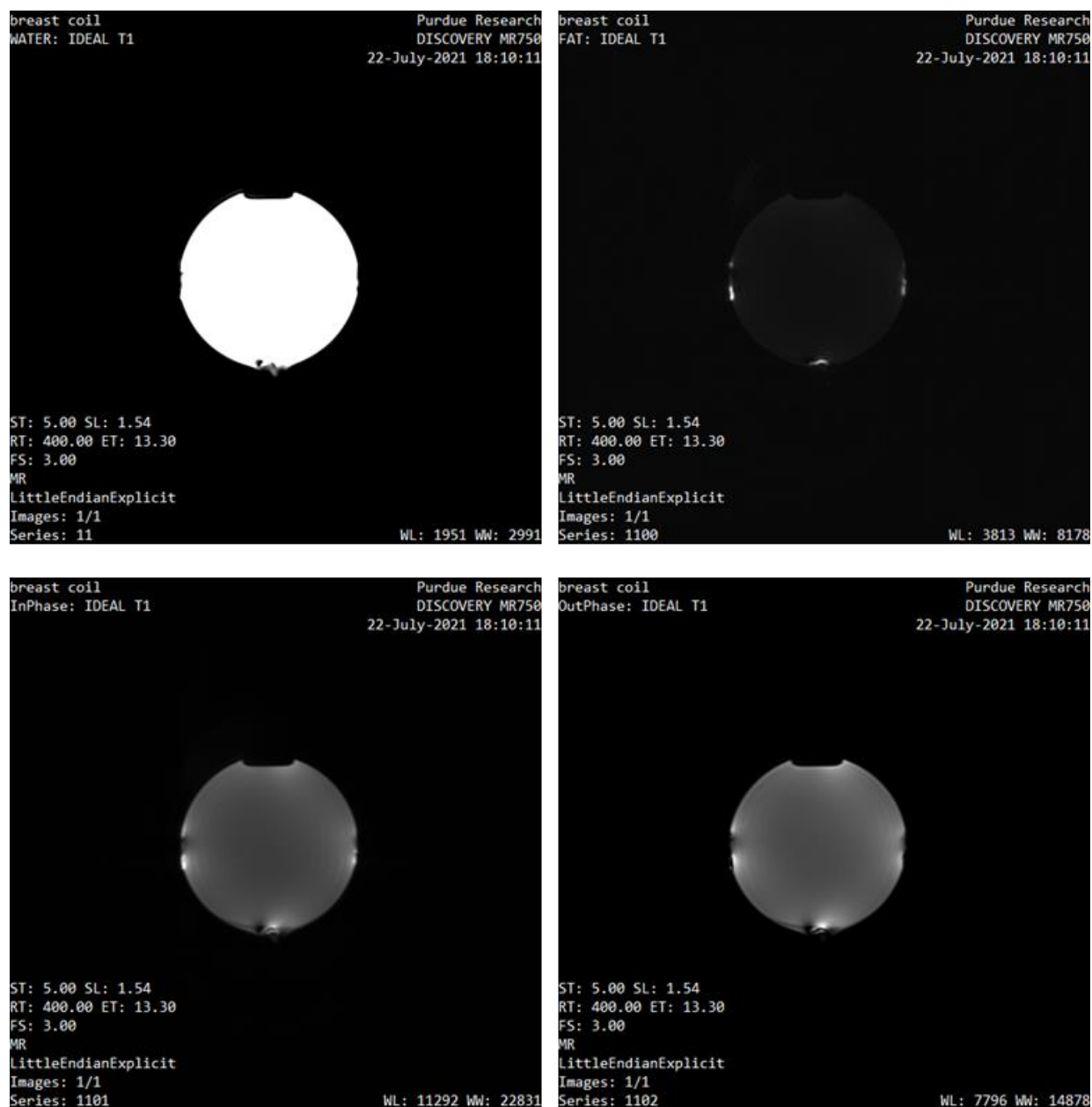


Figure 3.12 IDEAL T1-weighted MRI scan. Brightness and windowing were adjusted to accentuate the brightness near the coil. IDEAL sequence includes water only, fat only, in-phase, and out-of-phase sequences.

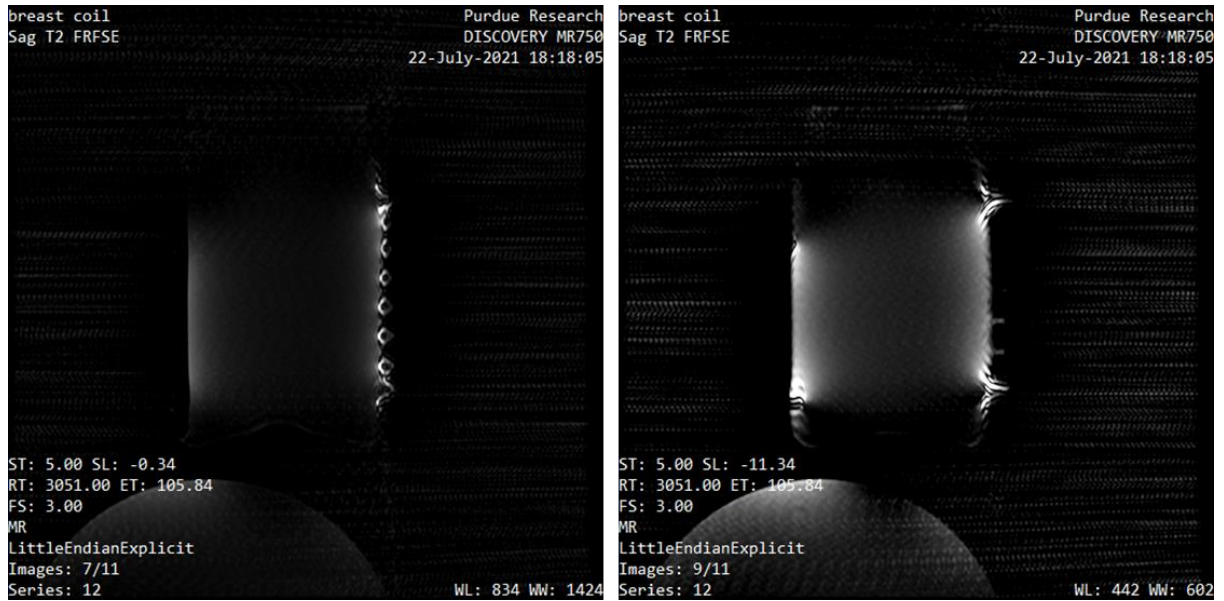


Figure 3.13 Sagittal T2-weighted MRI scan. Brightness and windowing were adjusted to accentuate the brightness near the coil.

Table 3.5 SNR calculations for axial T1, axial IDEAL, and sagittal T2-weighted images.

	Region of Noise	Region of Interest			SNR		
	Average	1	2	3	1	2	3
Axial T1	15.71	7097.61	5994.56	11452.42	451.86	381.64	729.11
IDEAL - Water only	23.46	6170.31	4954.86	10315.63	262.99	211.18	439.66
IDEAL - Fat only	14.44	362.44	253.14	1393.81	25.10	17.53	96.54
IDEAL - In-phase	22.22	184.01	5318.00	14367.58	8.28	239.33	646.61
IDEAL - Out-of-phase	16.53	5461.47	4567.39	12404.69	330.35	276.27	750.32
Sagittal T2	15.84	206.80	487.19	N/A	13.06	30.77	N/A

4. CONCLUSION

The peak-to-dip difference observed on the tuned and detuned states of the RF coil was excellent, as a difference of 35 dB is a target for clinical coils. All T1 and T2 weighted images also demonstrated sufficient signal acquisition from the phantom. Referring to Table 3.5, the SNR of all scanned images were excellent. It is understandable that the SNR is higher near the surface compared to the middle of the phantom as discussed on Figure 1.5 and 1.6.

The research has significance that the stretchable RF coil can be wearable easily for those who have difficulties to move their neck due to any types of disabilities. While the conventional cervical spine RF coil is uncomfortable for those with neck pain, as it is rigid and heavy, the novel stretchable RF coil has advantages of improved comfort and lightweight. The characteristic of being stretchable will allow the coil elements to nicely wrap around the subject's neck with hook-and-loop fastener. The proximity of the RF coil on the neck will increase the SNR as the coil is closer to the source compared to the conventional RF coil. It is also economically efficient that it is mainly composed of stretchable fabric and conductive thread.

This research can be extended by building more channels and modifying the design such as overlapped or geometrically decoupled array elements. The shape of the coil can also be modified to find the most efficient RF coil. Future works may include in vivo testing and stretchable RF coil on the joints, including ankle and wrist.

REFERENCES

1. GE Healthcare. (2018, August 6). *1.5T Compared to 3.0T MRI Scanners*. GE Healthcare. <https://www.gehealthcare.com/article/15t-compared-to-30t-mri-scanners>.
2. Lloyd-Jones, G. (2017, September). *MRI interpretation t1 v t2 images*. Radiology Masterclass. https://www.radiologymasterclass.co.uk/tutorials/mri/t1_and_t2_images.
3. Van der Plas, A. (2015, June 3). *MRI Technique*. Startradiology. <https://www.startradiology.com/the-basics/mri-technique/index.html>.
4. Murphy, A., & Ballinger, J. R. (n.d.). *Radiofrequency coils*. Radiopaedia. Retrieved June 30, 2021, from <https://radiopaedia.org/articles/radiofrequency-coils-1?lang=us>.
5. Gruber, B., Froeling, M., Leiner, T., & Klomp, D. W. J. (2018). RF coils: A practical guide for nonphysicists. *Journal of Magnetic Resonance Imaging*, 48(3), 590–604. <https://doi.org/10.1002/jmri.26187>
6. Wright, S. M., & Wald, L. L. (1997). Theory and application of array coils in mr spectroscopy. *NMR in Biomedicine*, 10(8), 394–410. [https://doi.org/10.1002/\(sici\)1099-1492\(199712\)10:8<394::aid-nbm494>3.0.co;2-0](https://doi.org/10.1002/(sici)1099-1492(199712)10:8<394::aid-nbm494>3.0.co;2-0)
7. Hingorjo, M. R., Qureshi, M. A., & Mehdi, A. (2012). Neck circumference as a useful marker of obesity: a comparison with body mass index and waist circumference. *JPM. The Journal of the Pakistan Medical Association*, 62(1), 36–40.
8. Han, T. S., Oh, M. K., Kim, S. M., Yang, H. J., Lee, B. S., Park, S. Y., & Lee, W. J. (2015). Relationship between Neck Length, Sleep, and Cardiovascular Risk Factors. *Korean Journal of Family Medicine*, 36(1), 10. <https://doi.org/10.4082/kjfm.2015.36.1.10>
9. Keil, B. “Construction of Receive Arrays,” *21st ISMRM: Weekend Educational Course*, April 20-26, 2013
10. Kajfez, D. (2005). Q-factor. *Encyclopedia of RF and Microwave Engineering*. <https://doi.org/10.1002/0471654507.eme333>
11. *Quality Factor*. Electronics Notes. (n.d.). Retrieved July 3, 2021, from https://www.electronics-notes.com/articles/basic_concepts/q-quality-factor/basics-tutorial-formula.php.
12. Gabriel, C. Compilation of the Dielectric Properties of Body Tissues at RF and Microwave Frequencies, Report N.AL/OE-TR- 1996-0037, Occupational and environmental health directorate, Radiofrequency Radiation Division, Brooks Air Force Base, Texas (USA), 1996.

13. Duan, Q., Duyn, J. H., Gudino, N., de Zwart, J. A., van Gelderen, P., Sodickson, D. K., & Brown, R. (2014). Characterization of a dielectric phantom for high-field magnetic resonance imaging applications. *Medical Physics*, 41(10), 102303. <https://doi.org/10.1118/1.4895823>
14. Mitchell, M. D., Kundel, H. L., Axel, L., & Joseph, P. M. (1986). Agarose as a tissue EQUIVALENT phantom material for NMR imaging. *Magnetic Resonance Imaging*, 4(3), 263–266. [https://doi.org/10.1016/0730-725x\(86\)91068-4](https://doi.org/10.1016/0730-725x(86)91068-4)
15. Schmid & Partner Engineering AG, DAK V 2.6 Professional Handbook, March 2020
16. GE Healthcare. (n.d.). *Image is Everything*. IDEAL. Retrieved July 22, 2021, from https://www.gehealthcare.com/-/jssmedia/widen/gehealthcarecom/migrated/chures-discovery-mr-750-3-0t-gehealthcare-brochure_discovery-mr750-image-is-everything_pdf.pdf?rev=-1&hash=E2395CFE564F80CFE8FA1175B15AD469.
17. Yang, X., Cui, Y., Yue, J., He, H., Yu, C., Liu, P., Liu, J., Ren, X., & Meng, Y. (2017). The histological characteristics, age-related thickness change of skin, and expression of the hsps in the skin during hair cycle in yak (*bos grunniens*). *PLOS ONE*, 12(5). <https://doi.org/10.1371/journal.pone.0176451>